Am J Transl Res 2022;14(4):2501-2526
www.ajtr.org /ISSN:1943-8141/AJTR0141940

Original Article

Integrated analyses of an RNA binding protein-based signature related to tumor immune microenvironment and candidate drugs in osteosarcoma

Abdulraheem Gul Mohammad[1*], Dapeng Li[1*], Rong He[2*], Xuan Lei[3*], Lianghao Mao[1], Bing Zhang[1], Xinyu Zhong[1], Zhengyu Yin[1], Wenbing Cao[1], Wenchao Zhang[1], Ruoxuan Hei[4], Qiping Zheng[4,5], Yiming Zhang[1]

[1]Department of Orthopedics, Affiliated Hospital of Jiangsu University, Zhenjiang 212001, Jiangsu, China; [2]Cancer Institute, The Affiliated People's Hospital of Jiangsu University, Zhenjiang 212000, Jiangsu, China; [3]Department of Burn and Plastic Surgery, Affiliated Hospital of Jiangsu University, Zhenjiang 212001, Jiangsu, China; [4]Department of Hematological Laboratory Science, Jiangsu Key Laboratory of Medical Science and Laboratory Medicine, School of Medicine, Jiangsu University, Zhenjiang 212000, Jiangsu, China; [5]Shenzhen Academy of Peptide Targeting Technology at Pingshan, and Shenzhen Tyercan Bio-Pharm Co., Ltd., Shenzhen 518118, Guangdong, China. [*]Equal contributors and co-first authors.

Received January 22, 2022; Accepted March 24, 2022; Epub April 15, 2022; Published April 30, 2022

Abstract: Objective: Osteosarcoma is the most frequent primary bone malignancy, associated with frequent recurrence and lung metastasis. RNA-binding proteins (RBPs) are pivotal in regulating several aspects of cancer biology. Nonetheless, interaction between RBPs and the osteosarcoma immune microenvironment is poorly understood. We investigated whether RBPs can predict prognosis and immunotherapy response in osteosarcoma patients. Methods: We constructed an RBP-related prognostic signature (RRPS) by univariate coupled with multivariate analyses and verified the independent prognostic efficacy of the signature. Single-sample Gene Set Enrichment Analysis (ssGSEA) along with ESTIMATE analysis were carried out to investigate the variations in immune characteristics between subgroups with various RRPS-scores. Furthermore, we investigatedpossible small molecule drugs using the connectivity map database and validated the expression of hub RBPs by qRT-PCR. Results: The RRPS, consisting of seven hub RBPs, was an independent prognostic factor compared to traditional clinical features. The RRPS could distinguish immune functions, immune score, stromal score, tumor purity and tumor infiltration by immune cells in different osteosarcoma subjects. Additionally, patients with high RRPS-scores had lower expression of immune checkpoint genes than patients with low RRPS-scores. We finally identified six small molecule drugs that may improve prognosis in osteosarcoma patients and substantiated notable differences in the contents of these RBPs. Conclusion: We evaluated the prognostic value and clinical application of an RBPs-based prognostic signature and identified promising biomarkers to predict immune cell infiltration and immunotherapy response in osteosarcoma.

Keywords: Osteosarcoma, RNA-binding protein, prognosis, immunotherapy, small molecule drugs

Introduction

Osteosarcoma is the most frequent primary bone cancer, most often affecting the epiphyses of the extremities, particularly the proximal tibia along with distal femur, with the greatest prevalence in children and teenagers [1, 2]. Osteosarcoma is associated with poor prognosis due to the frequency of recurrence and distant metastasis [3]. At diagnosis, 20% of the individuals with osteosarcoma already have pulmonary metastases, thus missing the optimal window for therapeutic intervention [4]. Surgical resection has been the standard of care for osteosarcoma patients since the 1970s, but the rate of long-term survival-was less than 20% at that time [5, 6]. In recent years, advances in surgical techniques and neoadjuvant chemotherapy have rgreatly enhanced the survival rate of osteosarcoma patients to approximately 60%-70% [7, 8]. Nevertheless, osteosarcoma patients still lack reliable early diagnostic indicators, and the five-year rate of survival of subjects with metastatic

osteosarcoma has consistently remained under 30% [9]. Critically, the development of targeted therapies for osteosarcoma is a significant-challenge due to intra-tumor and inter-individual heterogeneity [10]. Therefore, promising biomarkers for predicting immune infiltration, as well as response to immunotherapy in osteosarcoma need to be identified.

Immunotherapy, a novel therapeutic approach that stimulates or suppresses aspects of the human immune system, has recently become a widely used cancer treatment and can improve patient survival [11]. Because some patients are not responsive to immune checkpoint inhibitors (ICI), immunotherapy also requires identification of cancer-specific biomarkers for precise application [12]. The use of integrated genetic biomarkers to predict prognosis in osteosarcoma patients has been extensively reported. For example, a pyroptosis-related prognostic index has been documented- as an independent indicator of osteosarcoma prognosis [13]. Similarly, Zheng et al. [14] established a nine-gene signatureand they evaluated the relationship between risk score and chemosensitivity in osteosarcoma. However, effectiveness of combinatorial biomarkers on the basis of RNA-binding proteins (RBPs) in osteosarcoma has not been studied extensively.

RBPs constitute a class of proteins that crosstalk with diverse RNAs, including transfer RNAs, micro RNAs, small nucleolar RNAs, long noncoding RNAs, ribosomal RNAs, mRNAs, and small nuclear RNAs [15]. Recent research has identified RBPs as potent cellular and molecular homeostasis regulators, involved in almost all steps of posttranscriptional regulation, such as RNA splicing, stabilization, maturation, localization, transport, translation, editing, and chemical modifications [16]. RBPs may contribute to various phenotypes related to cancer development and progression by regulating target RNAs implicated in growth, apoptosis, infiltration, metastasis, and epithelial-mesenchymal transition (EMT) [17]. For example, insulin-like growth factor-2 mRNA-binding proteins (IGF2BPs) are involved in regulating the expression and function of classical oncogenes, such as KRAS, MDR1, and MYC, and are strongly associated with tumor aggressiveness and metastasis [18]. IGF2BP1 is commonly upregulated in most tumor tissues and contributes to the localization, translation, and stability of cancer-related mRNA targets by regulating some microRNAs and long non-coding RNAs [19]. Also, Guo et al. [21] found that upregulation of CUGBP elav-like family member 2 (CELF2) stabilized FAM198B, thereby inhibiting ovarian cancer progression, migration, and metastasis. Furthermore, CELF2 was positively correlated with progression-free survival (PFS) and overall survival (OS) of individuals with ovarian cancer. Collectively, these studies illustrate RBPs are tied to development and progression of multiple cancers. Therefore, an effective RBP-based genetic marker may indicate osteosarcoma prognosis and guide clinical treatment, especially the use of immunotherapy.

In this study, we downloaded gene expression data from the Therapeutically Applicable Research to Generate Effective Treatments (TARGET), Genotype-Tissue Expression (GTEx), as well as Gene Expression Omnibus (GEO) data resources for osteosarcoma and normal samples, along with clinical data from osteosarcoma patients. We screened multiple RBPs associated with osteosarcoma prognosis to construct an RBP-related prognostic signature (RRPS). We further discussed the possible value of RRPS in identifying immune microenvironment features and predicting immunotherapy response. Then, we validated the clinical application value of RRPS under different clinical parameters and screened some small molecule drugs. Finally, we assessed the prognostic worthiness of key RBPs and their expression in osteosarcoma cell lines through independent databases and qRT-PCR, respectively. Our results suggest the RBP-linked prognostic signature can be used as a new prognostic indicator for osteosarcoma that can predict immune cell infiltration and immunotherapeutic response in osteosarcoma.

Materials and methods

Data source and determination of differentially expressed RBPs

An overview of this study's workflow is presented in **Figure 1**. The RNA sequencing (RNA-seq) data for normal muscle tissue samples were abstracted from the GTEx data resource (https://www.gtexportal.org/home/). Gene ex-

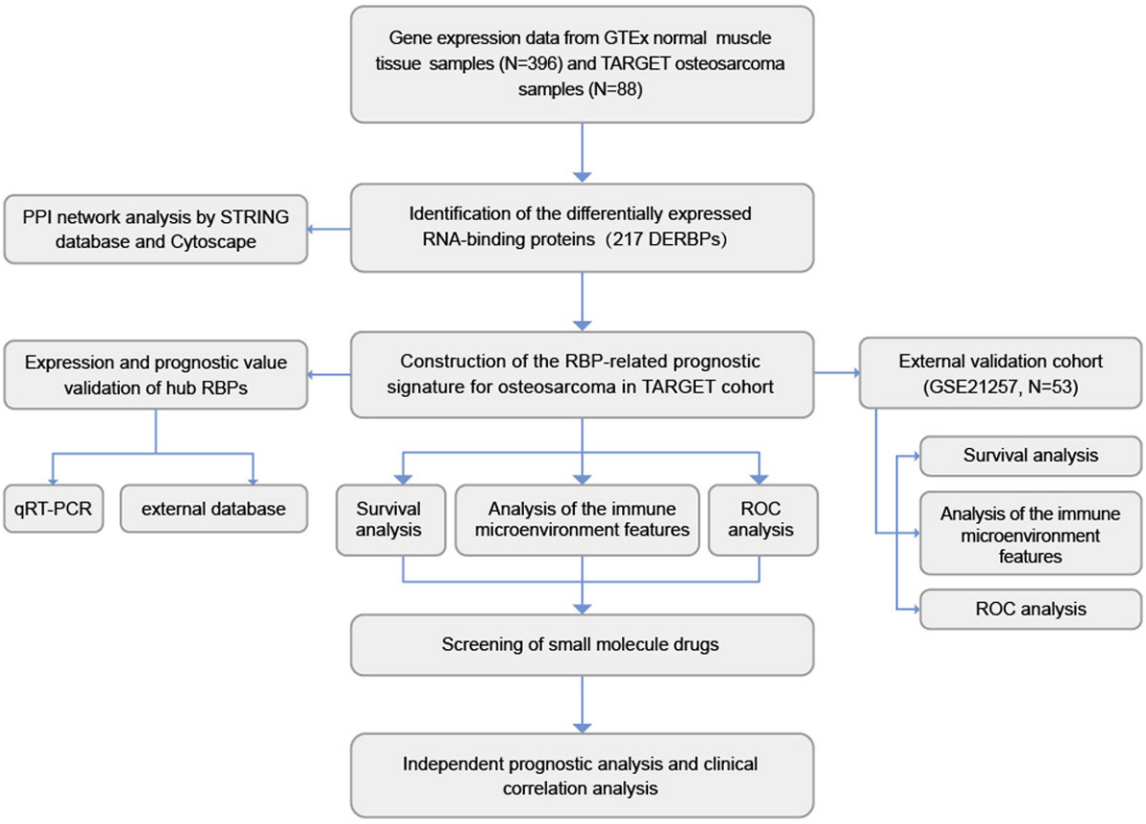

Figure 1. Flow chart of the study.

pression data along with corresponding data of the osteosarcoma samples were abstracted from TARGET data resource (https://ocg.cancer.gov/programs/target). A total of 484 samples were obtained, including 88 osteosarcoma samples and 396 non-tumorous samples (tumor samples were all from the TARGET data resource and non-tumorous samples were all from the GTEx data resource) [22, 23]. The list of 1542 RNA-binding proteins (RBPs) used to filter differentially expressed RBPs (DERBPs) is shown in Supplementary Table 1 [15]. The raw data were subsequently preprocessed through the "limma" package, and DERBPs were identified by a |log2 fold change (FC)| ≥ 1 along with false discovery rate (FDR) < 0.05. The microarray expression dataset GSE21257, which contains 53 osteosarcoma samples, was abstracted from the GEO data resource (http://www.ncbi.nlm.nih.gov/geo). TARGET cohort served as the training set, whereas the GSE21257 cohort served as the verification set.

GO and KEGG pathway enrichment analysis of DERBPS

To further determine the biologic functions of the identified differentially expressed RBPs, we performed Gene Ontology (GO) along with Kyoto Encyclopedia of Genes and Genomes (KEGG) pathways enrichment analysis. GO enrichment analysis consists of biological processes (BP), cellular components (CC), and molecular functions (MF). The packages "clusterProfiler", "org.Hs.eg.db", "ggplot2", and "enrichment plot" were used for annotation and visualization. FDR < 0.05 signified statistical significance.

Protein-protein interaction network construction and module screening

To predict protein-protein interactions between DERBPs, all DERBPs were imported into the Search Tool for the Retrieval of Interacting Genes (STRING) data resource (https://string-db.org/). We set the protein-protein cross-talk screening criterion as a minimum required

interaction score > 0.4. Then, we used Cytoscape (http://www.cytoscape.org/) for visual analysis of the protein-protein interaction (PPI) network. The plugin MCODE in Cytoscape was used to detect significant modules in the PPI network (cut-off = 2, haircut on, node score cutoff = 0.2, max depth = 100, k-score = 2, and score > 4), and the obtained modules were subjected to GO along with KEGG assessment to further assess their biologic functions and pathways in osteosarcoma (adjusted $P < 0.05$ served as the screening criterion).

Construction of a prognostic signature for osteosarcoma

On the basis of the DERBPs in the training cohort, we performed univariate Cox regression with the "survival" package to identify DERBPs linked to prognosis. Then, multivariate Cox regression was applied to determine the prognostic RBPs for our osteosarcoma prognostic signature. The RBP-linked prognostic signature score, which we designated as "RRPS-score" for every patient, was computed as follows: RRPS-score = $(coef_1 \times exp_1) + (coef_2 \times exp_2) + \ldots + (coef_x \times exp_x)$ (x designates the gene number in this model, exp designates the content of each gene, coef designates the coefficient value). Patients with osteosarcoma were then stratified into high-RBP and low-RBP scoring groups on the basis of the median RRPS-score. For survival assessment of the subgroups, plotting of the Kaplan-Meier survival curves was done via the "survival" and "survminer" packages. We adopted the time-dependent receiver operating characteristic (ROC) assessment of OS to assess the accuracy along with the sensitivity of the prognostic model by the "survivalROC" package. For survival assessment, a $P < 0.05$ and an area under ROC (AUC) > 0.60 was considered an acceptable predictive value. We also evaluated our model using an expression heat map of RBPs in the RRPS, RRPS-score, survival status, and the survival time distribution. Finally, alterations of copy-numbers coupled with mutation assessment of survival-associated RBPs in sarcoma was performed using the cBioportal data resource (http://www.cbioportal.org/).

Verification of the prognostic signature for osteosarcoma

A verification cohort of 53 osteosarcoma patient samples from the GSE21257 dataset with credible prognostic information was utilized to confirm the reliability of our prognostic signature.

Analysis of immune characteristics among subgroups

Single-sample Gene Set Enrichment Analysis (ssGSEA) was performed to explore immune cell invasion and activity of immune-linked cascades between high-RRPS and low-RRPS subgroups by applying the "gsva" package in the training, as well as the verification data sets. Patients with osteosarcoma in both subgroups were assessed for immune score, tumor purity, and stromal score using the "estimate" package. Expression of the immune checkpoint genes (*HAVCR2*, *PDL1*, *LAG3*, *TDO2*, *PDCD1*, *CTLA4*, *IDO1*, and *TIGIT*) was analyzed between low- and high-scoring groups using the "limma", "reshape2", "ggplot2", and "ggpubr" packages to estimate the response of osteosarcoma patients to ICI therapy.

Screening small molecule drugs

We identified differentially expressed genes (DEGs) between low-RRPS and high-RRPS subgroups using the "limma" package with FDR < 0.05 and $|\log2FC| \geq 0.5$. Based on these DEGs, we predicted possible small molecule drugs for osteosarcoma by the Cmap data resource (https://portals.broadinstitute.org/cmap/). Negative drug enrichment scores represented drugs with the ability to inhibit target gene expression, and they were considered candidate antitumor drugs [24]. The 3D structures of the candidate drugs were obtained from the Pubchem data resource (https://pubchem.ncbi.nlm.nih.gov/).

Independent prognostic analysis and construction of nomogram

To assess whether our osteosarcoma prognostic signature was independent of other clinical factors, we performed univariate along with-multivariate Cox regression analyses on the entire TARGET cohort using the "survival" package. A nomogram was created to predict survival rates of osteosarcoma patients at one-, three-, and five-years using the "survival" and "rms" package.

Clinical correlation analysis and prognostic value validation of hub RBPs

Using the TARGET cohort, patients were stratified into two groups on the basis of age (≤ 20 and > 20 years), sex (female and male), and M (M0 and M1). Correlations between the hub RBPs involved in the RRPS and the above clinical traits were assessed using the "beeswarm" package with $P < 0.05$ signifying statistical significance. External verification of the prognostic worthiness of RBPs was done utilizing the osteosarcoma microarray dataset from the R2 data resource (https://hgserver1.amc.nl/cgi-bin/r2/main.cgi).

Cell culture

The human osteoblast cell line (hFOB1.19) along with osteosarcoma cell lines (MG-63, MNNG/HOS, and U-20S) were acquired through the Cell Bank of the Chinese Academy of Sciences (Shanghai, China). MG-63 and MNNG/HOS cells were cultured in DMEM mixed with 10% FBS (Biological Industries, United States) and 1% penicillin/streptomycin. Osteoblasts were inoculated in DMEM/F12 containing 10% FBS and 1% penicillin/streptomycin, while U2OS cells were maintained in McCoy's 5A medium. We cultured the cells at 37°C along with 5% CO_2 conditions.

Clinical samples

Tumor and adjacent tissue samples were collected from six pairs of patients with osteosarcoma from the Affiliated Hospital of Jiangsu University. Informed consent was granted by every subject. Tissue samples were placed in liquid nitrogen for RNA extraction immediately after surgical resection. This study was approved by the Ethics Review Committee of Jiangsu University.

qRT-PCR assays

Total RNA from cells and tissues was extracted with RNA-easy™ Isolation Reagent (Vazyme Biotech Co., Ltd., Nanjing, China) and converted to cDNA with the PrimerScript reagent kit (Takara, Beijing, China). The comparative $2^{-\Delta\Delta Ct}$ approach was adopted to determine relative contents, and GAPDH served as the internal reference. Primer sequences for relevant genes are provided in Supplementary Table 2.

Statistical analysis

All statistical analyses were implemented in R software (v4.0.5). We expressed measured results as mean ± standard deviation (SD). We performed Student's t-tests or one-way ANOVA to determine differences between groups, with $P < 0.05$ signifying significance.

Results

Identification of DERBPs in osteosarcoma and normal tissues

We downloaded gene expression data from 396 control samples and 88 osteosarcoma samples. Expression discrepancies of 1432 RBPs between control muscle tissue samples and osteosarcoma samples are shown in **Figure 2A**, **2B**. Based on our established cut-off standards (FDR < 0.05 and $|log2FC| \geq 1$), 217 DERBPs were used in the subsequent study, including 97 downregulated and 120 upregulated RBPs (Supplementary Table 3).

Functional enrichment analysis of DERBPs

We performed GO annotation and KEGG pathway enrichment analysis to elucidate the functions and molecular mechanisms of the 217 DERBPs. Regarding the upregulated DERBPs, the most enriched BP were virus defense response, response to virus, hydrolysis of RNA phosphodiester link, and modulation of mRNA metabolic process. For CC enrichment, upregulated DERBPs were primarily involved in cytoplasmic ribonucleoprotein granules, cytoplasmic stress granules, along with ribonucleoprotein granules. Concerning MF, upregulated DERBPs were primarily enriched in double-stranded RNA docking, catalytic activity acting on RNA, and single-stranded RNA docking (**Figure 3A**). In the downregulated DERBPs, the BP terms include RNA splicing, mRNA splicing through the spliceosome, and RNA splicing through the transesterification reactions with bulged adenosine as nucleophile, among others (**Figure 3B**). Within the CC category, downregulated DERBPs were enriched in RNA polymerase II core complex, cytoplasmic ribonucleoprotein granules, ribonucleoprotein granules, and others (**Figure 3B**). For MF enrichment, downregulated DERBPs are primarily enriched in translation factor activity, mRNA 3'-UTR docking, RNA docking, catalytic activity,

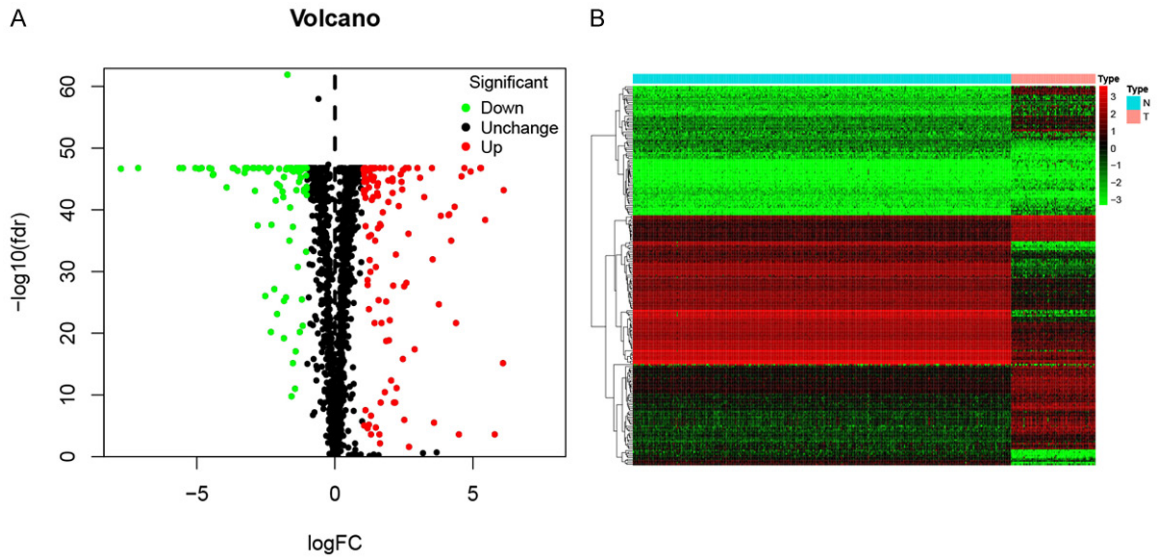

Figure 2. Identification of DERBPs in osteosarcoma. A. Volcano plot of DERBPs. B. Heatmap of DERBPs. DERBPs with upregulation, downregulation, and no significant difference were indicated by red, green, and black dots, respectively. T indicates tumor tissues, and N indicates non-tumor tissues. DERBPs, differentially expressed RNA-binding proteins.

along with acting on RNA (**Figure 3B**). Moreover, KEGG pathway enrichment assessment exhibited upregulated DERBPs were mainly enriched in influenza A, mRNA surveillance pathway, and coronavirus disease-COVID-19 (**Figure 3C**). In contrast, the downregulated DERBPs were very enriched in mRNA surveillance cascade, RNA transport, and legionellosis (**Figure 3D**).

Construction of PPI network and identification of critical modules

The PPI network of DERBPs was constructed using the STRING database, which includes 193 nodes and 637 edges (**Figure 4A**). Following this, four key modules were derived using the plugin MCODE (**Figure 4B**). Module 1, which is composed of 22 core proteins and 111 edges, gets the highest score among these clusters (**Figure 4C**). Module 2 consists of 6 nodes and 14 edges (**Figure 4D**), module 3 consists of 12 nodes and 22 edges (**Figure 4E**), and module 4 consists of 5 nodes and 8 edges (**Figure 4F**). The results of GO along with KEGG enrichment assessment for the RBPs in the sub-networks are shown in Supplementary Table 4.

Creation and verification of a seven-RBP signature for osteosarcoma

To identify survival-associated DERBPs, we extracted expression and survival information from the TARGET data resource and identified 13 prognosis-associated RBPs using univariate Cox regression analysis (**Figure 5A**). Afterwards, we performed multivariate Cox regression-based on these 13 prognosis-linked RBPs. Following this analysis, seven RBPs were retained and utilized to create the RRPS (**Figure 5B**). The seven-RBP genes are yrdC N6-threonylcarbamoltransferase domain containing (*YRDC*), zinc finger CCCH-type containing, antiviral 1 (*ZC3HAV1*), telomerase reverse transcriptase (*TERT*), RNA-binding motif protein 34 (*RBM34*), toll-like receptor 8 (*TLR8*), insulin-like growth factor 2 mRNA-binding protein-2 (*IGF2BP2*), and nuclear transport factor 2 like export factor 2 (*NXT2*). Among these, *YRDC*, *ZC3HAV1*, *TERT*, *RBM34*, and *IGF2BP2* were classified as high-risk genes on the basis of their hazard ratio (HR), whereas *TLR8* and *NXT2* were classified as low-risk genes (**Figure 5B**). The RRPS-score formula consisting of seven RBPs is as follows: RRPS-score = (0.8638 × level of expression of *YRDC*) + (0.8321 × level of expression of *ZC3HAV1*) + (0.8503 × level of expression of *TERT*) + (1.0753 × level of expression of *RBM34*) + (-1.4991 × level of expression of *TLR8*) + (0.3633 × level of expression of *IGF2BP2*) + (-0.2851 × expression level of *NXT2*). We conducted a survival analysis to assess the predictive power of the RRPS. Osteosarcoma patients in the training set were classified into low and

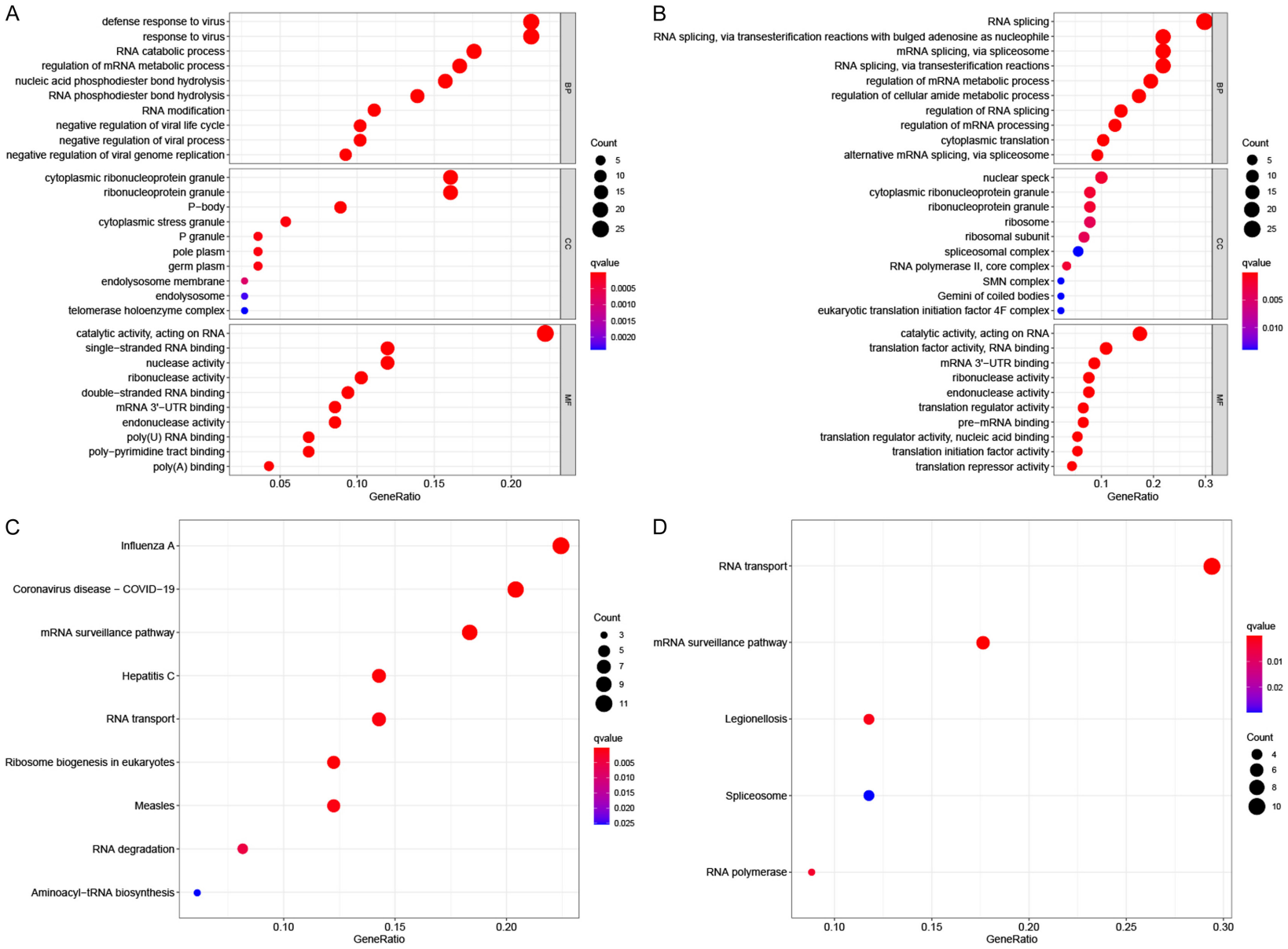
A
defense response to virus
response to virus
RNA catabolic process
regulation of mRNA metabolic process
nucleic acid phosphodiester bond hydrolysis
RNA phosphodiester bond hydrolysis
RNA modification
negative regulation of viral life cycle
negative regulation of viral process
negative regulation of viral genome replication
cytoplasmic ribonucleoprotein granule
ribonucleoprotein granule
P−body
cytoplasmic stress granule
P granule
pole plasm
germ plasm
endolysosome membrane
endolysosome
telomerase holoenzyme complex
catalytic activity, acting on RNA
single−stranded RNA binding
nuclease activity
ribonuclease activity
double−stranded RNA binding
mRNA 3'−UTR binding
endonuclease activity
poly(U) RNA binding
poly−pyrimidine tract binding
poly(A) binding
BP
CC
MF
0.05
0.10
0.15
0.20
GeneRatio
Count
5
10
15
20
25
qvalue
0.0005
0.0010
0.0015
0.0020
B
RNA splicing
RNA splicing, via transesterification reactions with bulged adenosine as nucleophile
mRNA splicing, via spliceosome
RNA splicing, via transesterification reactions
regulation of mRNA metabolic process
regulation of cellular amide metabolic process
regulation of RNA splicing
regulation of mRNA processing
cytoplasmic translation
alternative mRNA splicing, via spliceosome
nuclear speck
cytoplasmic ribonucleoprotein granule
ribonucleoprotein granule
ribosome
ribosomal subunit
spliceosomal complex
RNA polymerase II, core complex
SMN complex
Gemini of coiled bodies
eukaryotic translation initiation factor 4F complex
catalytic activity, acting on RNA
translation factor activity, RNA binding
mRNA 3'−UTR binding
ribonuclease activity
endonuclease activity
translation regulator activity
pre−mRNA binding
translation regulator activity, nucleic acid binding
translation initiation factor activity
translation repressor activity
BP
CC
MF
0.1
0.2
0.3
GeneRatio
Count
5
10
15
20
25
qvalue
0.005
0.010
C
Influenza A
Coronavirus disease − COVID−19
mRNA surveillance pathway
Hepatitis C
RNA transport
Ribosome biogenesis in eukaryotes
Measles
RNA degradation
Aminoacyl−tRNA biosynthesis
0.10
0.15
0.20
GeneRatio
Count
3
5
7
9
11
qvalue
0.005
0.010
0.015
0.020
0.025
D
RNA transport
mRNA surveillance pathway
Legionellosis
Spliceosome
RNA polymerase
0.10
0.15
0.20
0.25
0.30
GeneRatio
qvalue
0.01
0.02
Count
4
6
8
10

Figure 3. GO and KEGG enrichment analysis of differentially expressed RBPs (DERBPs) in osteosarcoma. (A, B) GO enrichment analysis of upregulated DERBPs (A) and downregulated DERBPs (B). (C, D) KEGG pathway enrichment analysis of upregulated DERBPs (C) and downregulated DERBPs (D). DERBPs, differentially expressed RNA-binding proteins.

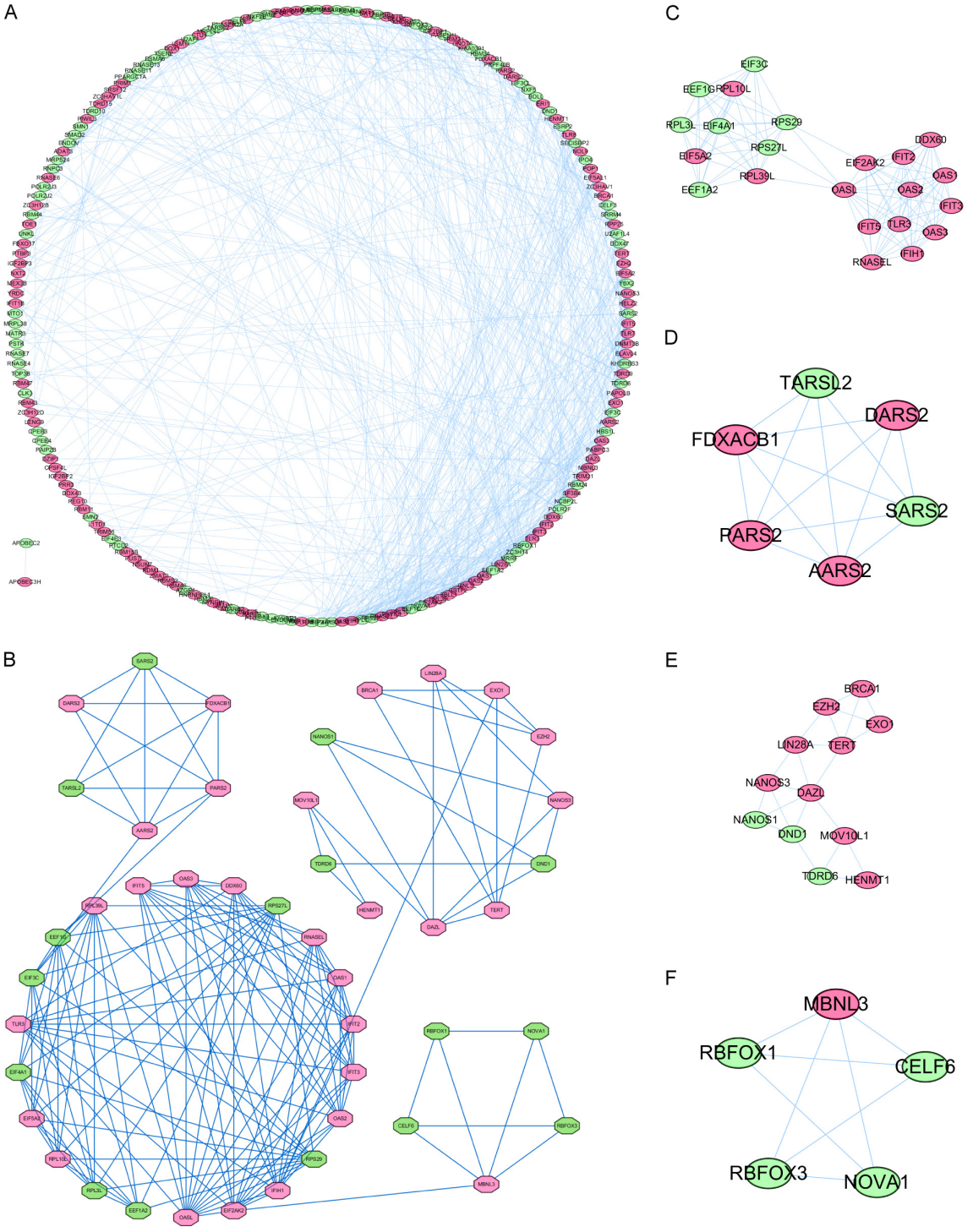

Figure 4. PPI network and module analysis of RBPs. (A) PPI network of DERBPs. (B) Visualization of four key modules. (C-F) Core modules in the PPI network. (C) module 1, (D) module 2, (E) module 3, and (F) module 4. The red nodes represent upregulated DERBPs, and the green nodes represent downregulated DERBPs. DERBPs, differentially expressed RNA-binding proteins.

A

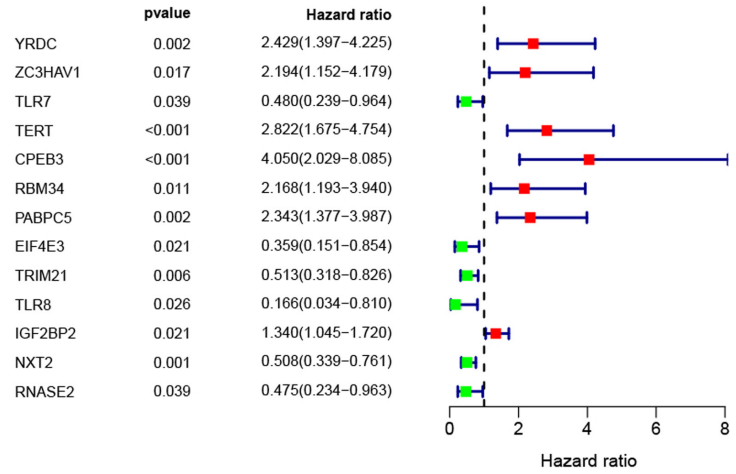
pvalue
Hazard ratio
YRDC 0.002 2.429(1.397−4.225)
ZC3HAV1 0.017 2.194(1.152−4.179)
TLR7 0.039 0.480(0.239−0.964)
TERT <0.001 2.822(1.675−4.754)
CPEB3 <0.001 4.050(2.029−8.085)
RBM34 0.011 2.168(1.193−3.940)
PABPC5 0.002 2.343(1.377−3.987)
EIF4E3 0.021 0.359(0.151−0.854)
TRIM21 0.006 0.513(0.318−0.826)
TLR8 0.026 0.166(0.034−0.810)
IGF2BP2 0.021 1.340(1.045−1.720)
NXT2 0.001 0.508(0.339−0.761)
RNASE2 0.039 0.475(0.234−0.963)
0 2 4 6 8
Hazard ratio

B

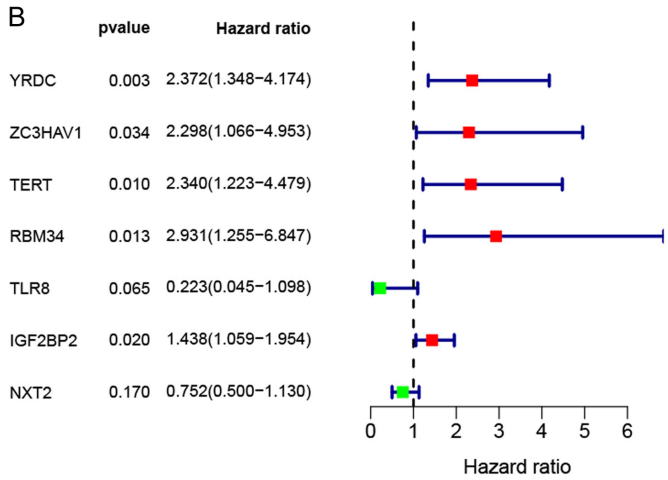
pvalue
Hazard ratio
YRDC 0.003 2.372(1.348−4.174)
ZC3HAV1 0.034 2.298(1.066−4.953)
TERT 0.010 2.340(1.223−4.479)
RBM34 0.013 2.931(1.255−6.847)
TLR8 0.065 0.223(0.045−1.098)
IGF2BP2 0.020 1.438(1.059−1.954)
NXT2 0.170 0.752(0.500−1.130)
0 1 2 3 4 5 6
Hazard ratio

C

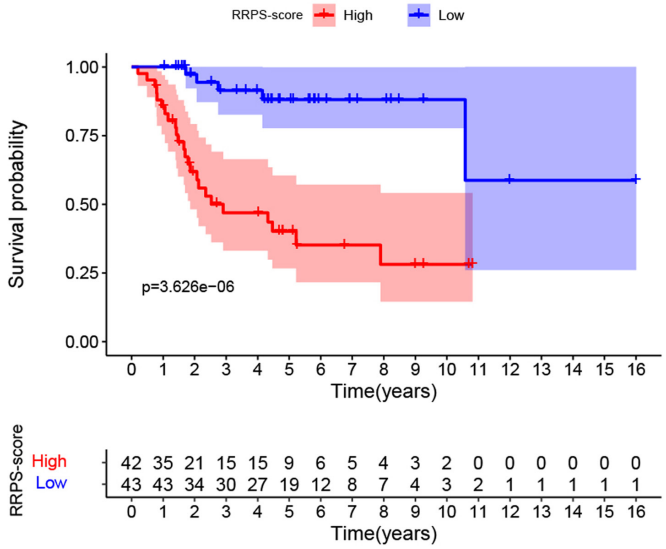
RRPS-score High Low
Survival probability
1.00 0.75 0.50 0.25 0.00
p=3.626e−06
0 1 2 3 4 5 6 7 8 9 10 11 12 13 14 15 16
Time(years)
RRPS-score
High 42 35 21 15 15 9 6 5 4 3 2 0 0 0 0 0 0
Low 43 43 34 30 27 19 12 8 7 4 3 2 1 1 1 1 1
0 1 2 3 4 5 6 7 8 9 10 11 12 13 14 15 16
Time(years)

D

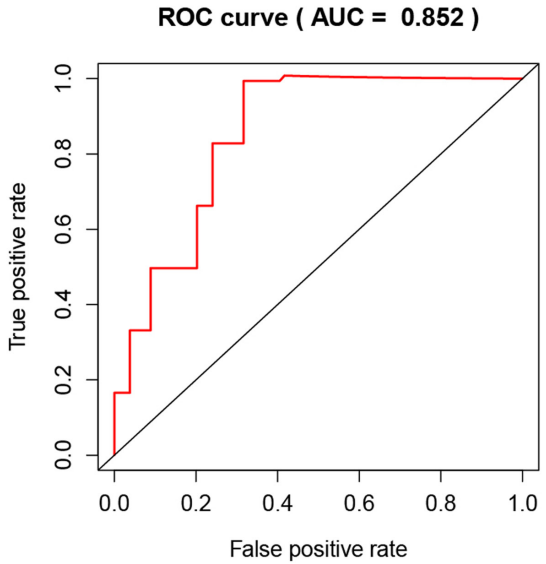
ROC curve (AUC = 0.852)
True positive rate
0.0 0.2 0.4 0.6 0.8 1.0
0.0 0.2 0.4 0.6 0.8 1.0
False positive rate

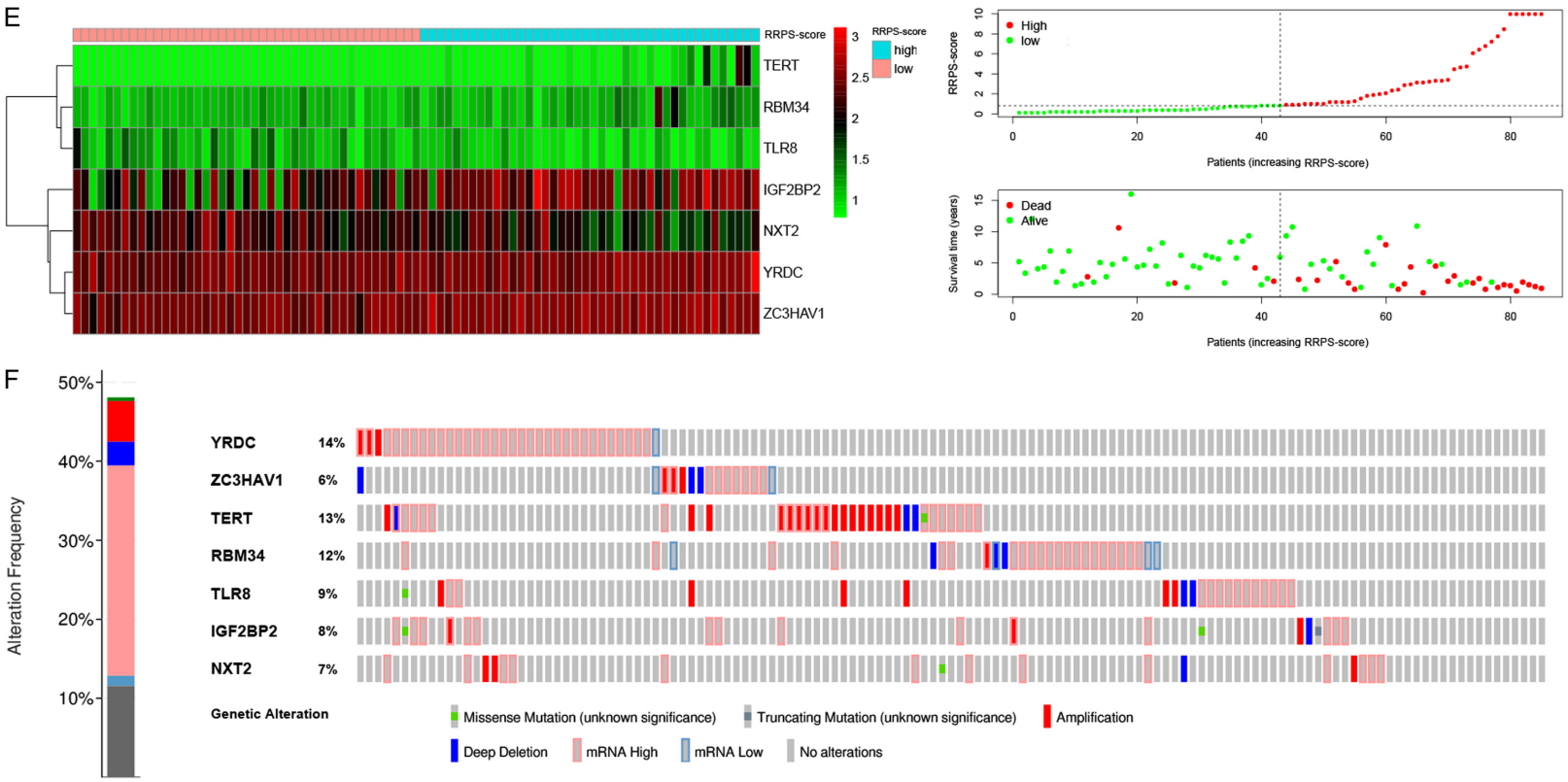

Figure 5. Creation and evaluation of a seven-RBP signature for osteosarcoma. (A, B) Identification of candidate prognosis-associated RBPs using univariate Cox regression analysis (A) and multivariate Cox regression analysis (B). (C) Survival analysis according to RRPS-score in the training cohort. (D) ROC curve for forecasting overall survival in the training cohort. (E) Expression heatmap of the seven RBPs, RRPS-score distribution, survival status, and survival time of patients in the training cohort. (F) Genomic alterations of the seven prognosis-related RBPs.

high RRPS-score groups on the basis of-median RRPS-score obtained from the above formula. Our results demonstrated overall survival was significantly inferior in patients with high RRPS-scores in contrast with those with low RRPS-scores (**Figure 5C**). Moreover, the area under the ROC curve (AUC) of the seven-gene signature was 0.852, which confirmed the prognostic value of RRPS (**Figure 5D**). **Figure 5E** shows the heatmap of expression of the seven RBPs in the training group as well as the distribution of RRPS-scores, survival status, and survival time of the patients. In conclusion, these data suggest RRPS has reliable predictive performance. We performed combined analysis of 7 prognosis-related RBPs mutations and copy-number alterations using cBioPortal. The results revealed these seven RBPs were altered in 115 out of 241 samples (48%), and several genes had copy number amplification, deep deletion, and increased mRNA levels (**Figure 5F**).

External validation of prognostic signature for osteosarcoma

To verify the reliability of our prognostic signature, we examined 53 osteosarcoma patients from the GSE21257 dataset as a verification cohort to assess the prognostic ability of RRPS. Patients in the GSE21257 cohort were categorized into high-RRPS and low-RRPS groups based on the median RRPS-score obtained from the above formula as a cut-off. As illustrated in **Figure 6A**, OS of the high RRPS-score group was lower in contrast to the low RRPS-score group. The result of the survival analysis in this external validation cohort was similar to the training cohort. Also, the ROC curve showed relatively good performance with the AUC of 0.684 for the RRPS in the validation cohort (**Figure 6B**). **Figure 6C** displays the expression heatmap of seven prognosis-related RBPs, RRPS-score, survival status, and survival time for osteosarcoma patients in the validation cohort. The above results indicate the RRPS-score can predict prognosis with sensitivity and specificity.

The RRPS-score is relevant to immune characteristics in osteosarcoma

We compared the immune characteristics of high and low-scoring RRPS subgroups by examining the level of immune cell infiltration, and the activity of immune-linked functions in the TARGET and GEO cohorts. In the TARGET cohort, the level of immune cell infiltration, specifically neutrophils, CD8 + T cells, regulatory T cells (Tregs), dendritic cells (DCs), T follicular helper (Tfh) cells, macrophages, T helper (Th) cells, along with tumor-infiltrating lymphocytes (TILs), and was generally decreased in the high-scoring subgroup in contrast to the low-scoring subgroup (**Figure 7A**). Only immature DC (iDC) infiltration was higher in the high RRPS-score sub-group than in the low RRPS-score subgroup (**Figure 7A**). All ten immune-related functions, including type I, and type II interferon (IFN) response pathways, were all significantly downregulated in the high RRPS-score subgroup with the exception of T cell co-stimulation (**Figure 7B**). In the GEO cohort, immune cell infiltration levels, such as activated DCs (aDCs), CD8 + T cells, DCs, mast cells, neutrophils, plasmacytoid dendritic cells (pDCs), Tfh cells, Th2 cells, and TILs, were similarly downregulated in the high RRPS-score subgroup (**Figure 7C**). Only the enrichment score of natural killer cells was significantly increased in the high-scoring subgroup (**Figure 7C**). In addition, twelve immune-related impaired functions were shown in addition to the type II IFN response in the high RRPS-score subgroup in the GEO cohort (**Figure 7D**). Our investigation revealed RRPS-score was linked to the level of immune infiltration in osteosarcoma. This result suggests elevated immune activity in the low RRPS-score group may contribute to the antitumor effect. Then, we further evaluated the value of the RRPS-score in the immune microenvironment of osteosarcoma with the ESTIMATE algorithm. We observed that the low RRPS-score subgroup had higher immune, stromal, and ESTIMATE scores, whereas the high RRPS-score subgroup had higher tumor purity (**Figure 7E-H**).

In addition, we analyzed the expression of the immune checkpoint genes to assess the ability of RRPS to predict response to ICI therapy in osteosarcoma patients. In the TARGET cohort, our results indicated expression levels of *LAG3*, *TIGIT*, *HAVCR2*, and *TDO2* were distinct in the different subgroups, and the expression of the immune checkpoint genes tended to be higher in the low RRPS-score group (**Figure 8A-H**). We also noted an inverse relationship of the RRPS-score with the expression of *TIGIT*,

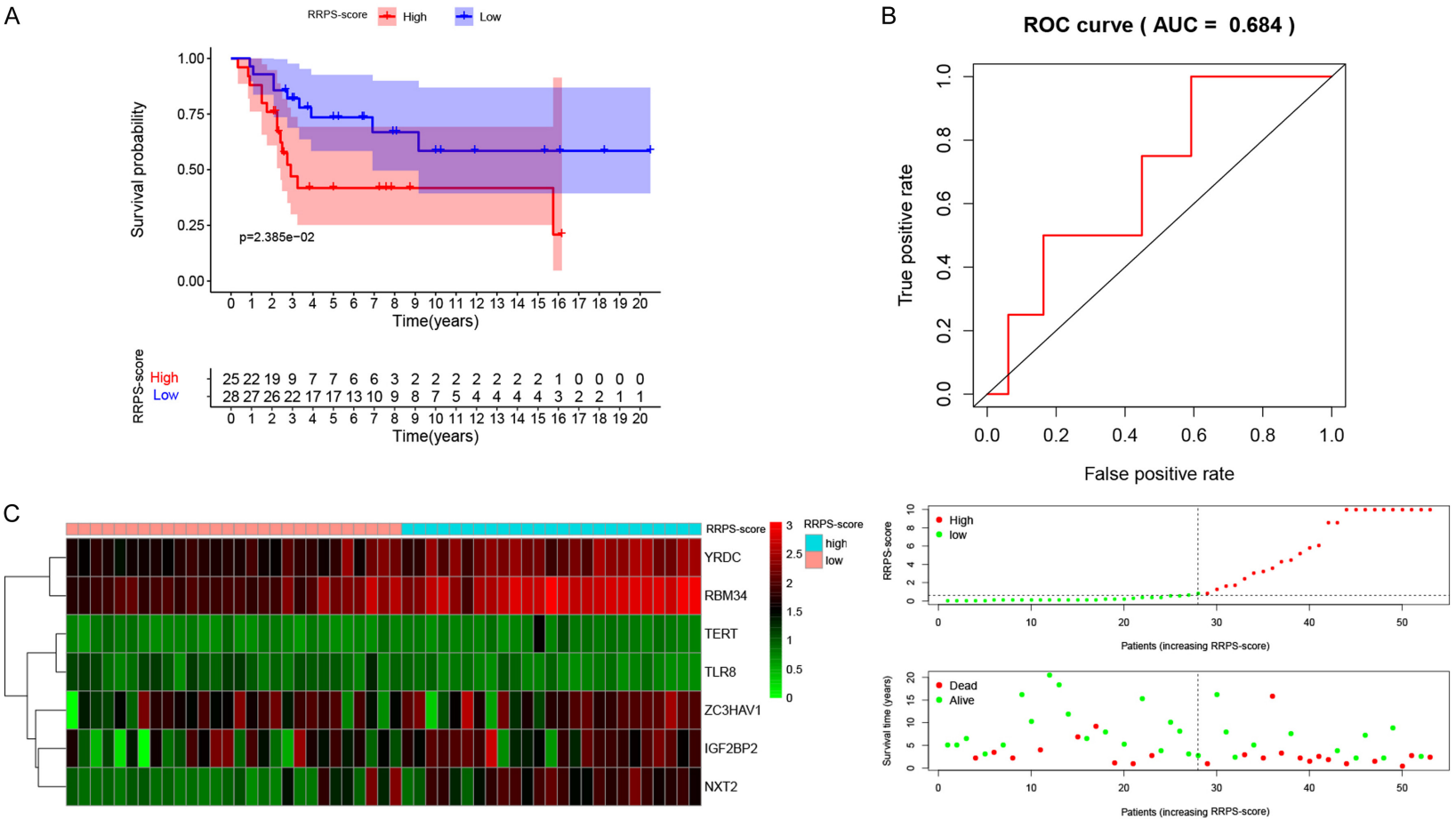

Figure 6. Verification of the prognostic signature for osteosarcoma. A. Survival analysis according to RRPS-score in the verification cohort. B. ROC curves for forecasting overall survival in the verification cohort. C. Expression heatmap of the seven RBPs, RRPS-score distribution, survival status, and survival time of the patients in the verification cohort.

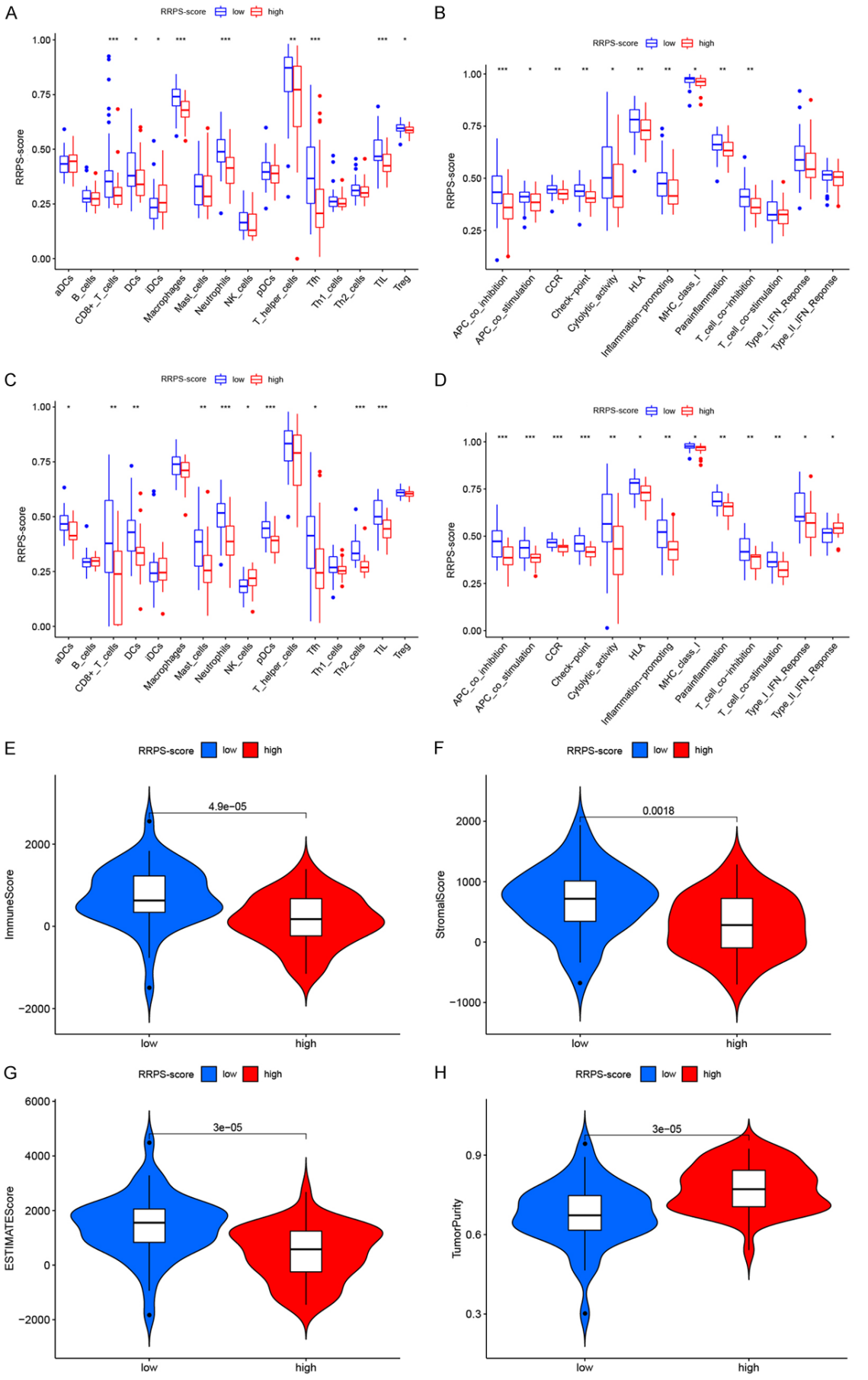
A
RRPS-score low high
RRPS-score
aDCs
B_cells
CD8+_T_cells
DCs
iDCs
Macrophages
Mast_cells
Neutrophils
NK_cells
pDCs
T_helper_cells
Tfh
Th1_cells
Th2_cells
TIL
Treg
B
RRPS-score low high
RRPS-score
APC_co_inhibition
APC_co_stimulation
CCR
Check-point
Cytolytic_activity
HLA
Inflammation-promoting
MHC_class_I
Parainflammation
T_cell_co-inhibition
T_cell_co-stimulation
Type_I_IFN_Reponse
Type_II_IFN_Reponse
C
RRPS-score low high
RRPS-score
D
RRPS-score low high
RRPS-score
E
RRPS-score low high
4.9e−05
ImmuneScore
low
high
F
RRPS-score low high
0.0018
StromalScore
low
high
G
RRPS-score low high
3e−05
ESTIMATEScore
low
high
H
RRPS-score low high
3e−05
TumorPurity
low
high

Figure 7. Immune characteristics of different RRPS-score subgroups. A. Disparities in immune cell infiltration between different subgroups in the TARGET set. B. Disparities in immune functions between different subgroups in the TARGET set. C. Disparities in immune cell infiltration between different subgroups in the GEO set. D. Disparities in immune functions between different subgroups in the GEO set. E. Comparative immune scores between different RRPS-score subgroups. F. Comparative stromal scores between different RRPS-score subgroups. G. Comparative ESTIMATE scores between different RRPS-score subgroups. H. Comparativetumor purity between different RRPS-score subgroups. The asterisks represent the statistical *P*-value; *P < 0.05; **P < 0.01; ***P < 0.001.

HAVCR2, and *TDO2* in the GEO cohort (**Figure 8I-P**). The above results suggest RRPS may be instrumental in understanding the characteristics of the immune microenvironment in osteosarcoma patients and may provide critical insights for individualized immunotherapy.

Independent prognostic value of the seven-rbp signature

We adopted univariate along with the multivariate Cox regression analyses to screen clinical characteristics linked to prognosis, such as gender, age, metastasis, and RRPS-score, to check whether our prognostic signature was independent of other clinical parameters. The data of the univariate assessment showed that RRPS-score (HR = 1.095, 95% CI = 1.059-1.132, P < 0.001) was strongly related to the OS of osteosarcoma patients (**Figure 9A**). In addition, metastasis was also a risk factor for osteosarcoma patients (**Figure 9A**). The data of the multivariate assessment exhibited that both metastasis and RRPS-score were independent predictors associated with OS of osteosarcoma patients (**Figure 9B**). Next, we created the nomogram based on the RRPS for predicting the OS of osteosarcoma patients at one-, three-, and five years. The scores corresponding to the seven RBPs were summed to calculate the total score for the patient and subsequently converted to obtain the probability of OS at one-, three-, and five years (**Figure 9C**).

Clinical utility and prognostic value of hub RBPs

We performed a clinical utility analysis of the hub RBPs involved in our prognostic signature (Supplementary Table 5). Patients with osteosarcoma metastases expressed higher levels of *YRDC* than patients without metastases (**Figure 10A**, P < 0.05). Conversely, patients with non-metastatic osteosarcoma had higher levels of *NXT2* expression (**Figure 10B**, P < 0.05). Besides, we examined expression between an older and younger group and found that the expression of *TERT* (**Figure 10C**, P < 0.01) and *RBM34* (**Figure 10D**, P < 0.05) was significantly higher in the younger group. Next, we used the R2 data resource to detect the prognostic worthiness of seven pivotal RBPs in osteosarcoma. The results illustrated that higher expression of *YRDC*, *TERT*, *RBM34*, and *NXT2* was linked to shorter OS time in osteosarcoma patients, whereas upregulated *TLR8* content was linked to favorable OS time in osteosarcoma patients (**Figure 11A-G**). In addition, expression levels of *TERT* and *RBM34* were negatively associated with metastasis-free survival (MFS) probability. Conversely, expression of *ZC3HAV1* and *TLR8* was positively associated with MFS in osteosarcoma patients (**Figure 11H-N**).

Small molecular drugs for osteosarcoma

As shown in Supplementary Table 6, we identified DEGs between the high and low RRPS-score subgroups, which included 69 upregulated genes and 94 downregulated genes. Based on these DEGs, we used the Cmap database to screen the six most significant small molecule drugs that may be useful for osteosarcoma treatment (**Table 1**). The 3D structures of the six small molecule drugs are shown in **Figure 12**.

Expression verification of seven hub RBP genes

The mRNA expression of these seven key RBP genes in osteosarcoma cell lines is shown in **Figure 13**. The results showed *YRDC* and *TERT* were over-expressedin all three osteosarcoma cell lines relative to hFOB 1.19 (**Figure 13A**, **13B**). On the contrary, the contents of *RBM34* and *IGF2BP2* were decreased in each osteosarcoma cell line (**Figure 13C**, **13D**). *ZC3HAV1*, *NXT2*, and *TLR8* were highly expressed in MNNG/HOS and U2OS but lowly expressed in MG-63 cell lines (**Figure 13E-G**). However, the contents of TERT and TLR8 in the tissues were

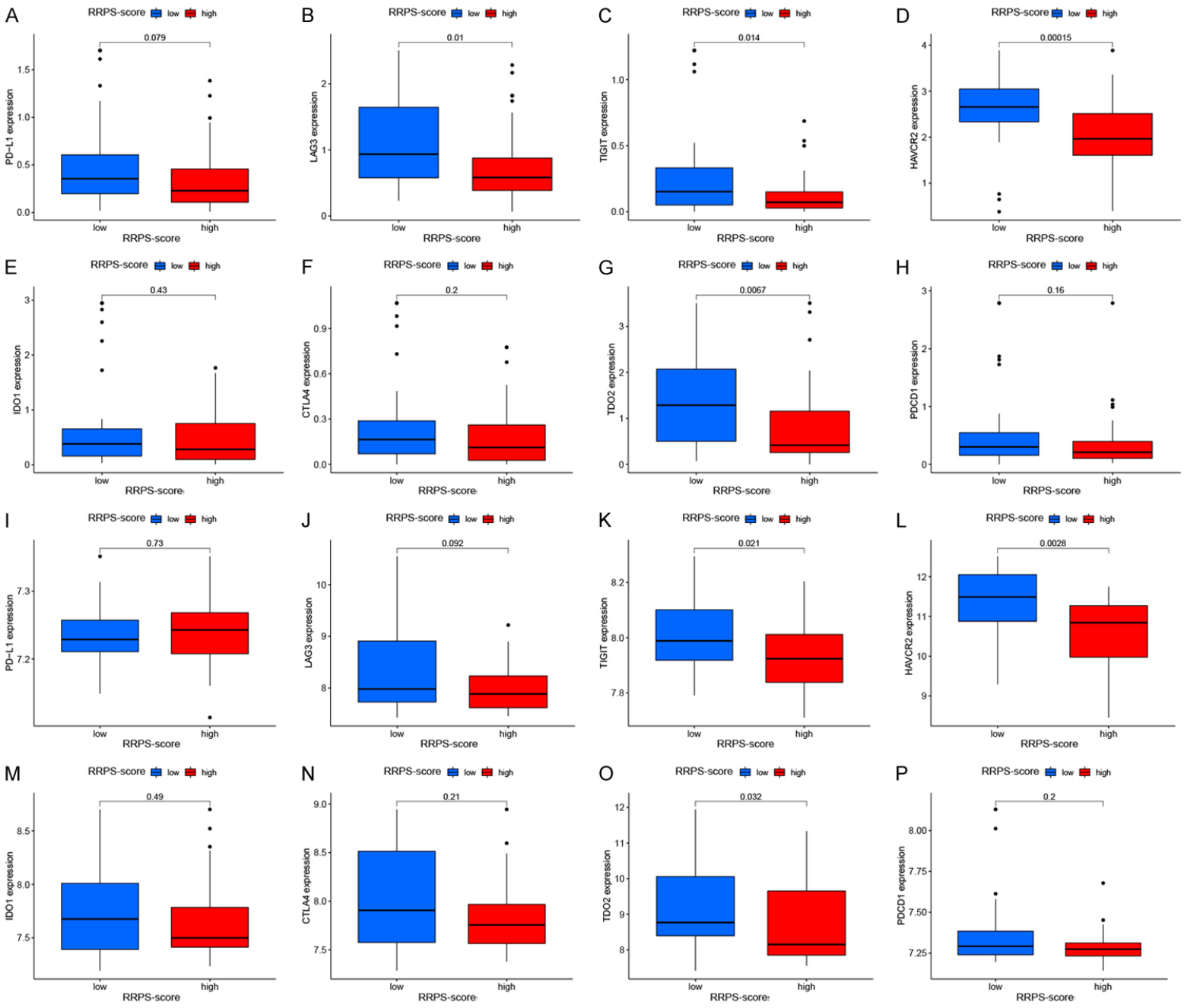
A
RRPS-score low high
0.079
PD−L1 expression
low high
RRPS-score
B
RRPS-score low high
0.01
LAG3 expression
low high
RRPS-score
C
RRPS-score low high
0.014
TIGIT expression
low high
RRPS-score
D
RRPS-score low high
0.00015
HAVCR2 expression
low high
RRPS-score
E
RRPS-score low high
0.43
IDO1 expression
low high
RRPS-score
F
RRPS-score low high
0.2
CTLA4 expression
low high
RRPS-score
G
RRPS-score low high
0.0067
TDO2 expression
low high
RRPS-score
H
RRPS-score low high
0.16
PDCD1 expression
low high
RRPS-score
I
RRPS-score low high
0.73
PD−L1 expression
low high
RRPS-score
J
RRPS-score low high
0.092
LAG3 expression
low high
RRPS-score
K
RRPS-score low high
0.021
TIGIT expression
low high
RRPS-score
L
RRPS-score low high
0.0028
HAVCR2 expression
low high
RRPS-score
M
RRPS-score low high
0.49
IDO1 expression
low high
RRPS-score
N
RRPS-score low high
0.21
CTLA4 expression
low high
RRPS-score
O
RRPS-score low high
0.032
TDO2 expression
low high
RRPS-score
P
RRPS-score low high
0.2
PDCD1 expression
low high
RRPS-score

Figure 8. Analysis of immune checkpoint expression between different RRPS-score subgroups. (A-H) Differential expression of immune checkpoint genes between the two subgroups in the TARGET set, including *PD-L1* (A), *LAG3* (B), *TIGIT* (C), *HAVCR2* (D), *IDO1* (E), *CTLA4* (F), *TDO2* (G), and *PDCD1* (H). (I-P) Differential expression of immune checkpoint genes between the two subgroups in the GEO set, including *PD-L1* (I), *LAG3* (J), *TIGIT* (K), *HAVCR2* (L), *IDO1* (M), *CTLA4* (N), *TDO2* (O), and *PDCD1* (P).

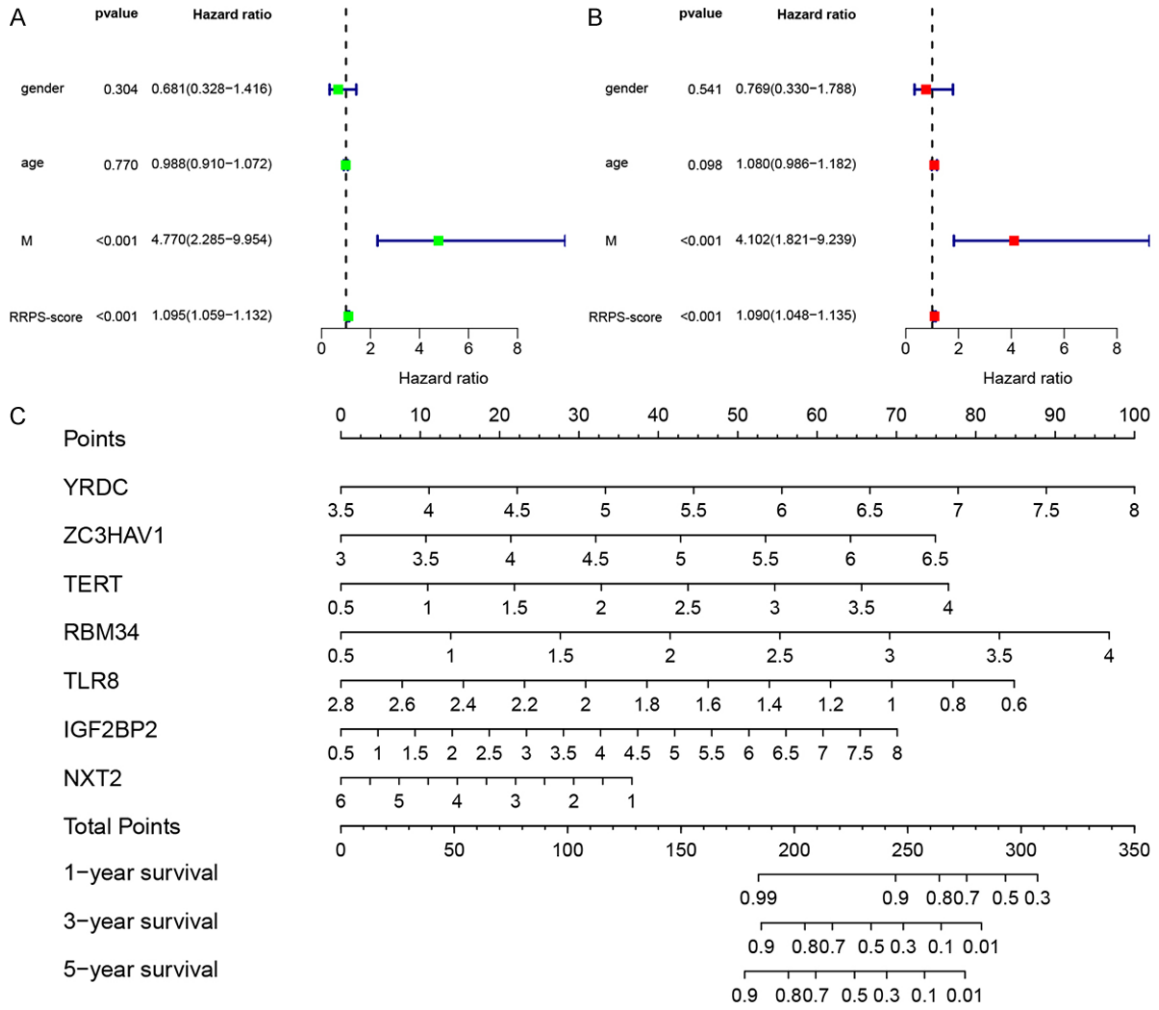

Figure 9. Prognostic value of different clinical parameters and creation of nomogram. A. Univariate regression analysis of various clinical parameters and RRPS-score in osteosarcoma patients. B. Multivariate regression analysis of various clinical data and RRPS-score in osteosarcoma patients. C. A seven-RBP based nomogram for predicting survival in osteosarcoma patients.

extremely low, and considering the humble confidence of qRT-PCR results, we determined relative contents of the remaining RBPs. As shown in **Figure 13H-L**, YRDC, ZC3HAV1, NXT2, and IGF2BP2 were highly expressed in osteosarcoma relative to control tissues, while RBM34 was lowly expressed in osteosarcoma.

Discussion

Osteosarcoma is the most frequent primary malignant bone tumor, which is linked to high mortality due to its association with metastasis, recurrence, and drug resistance [25, 26]. The absence of prognostic biomarkers to assess disease progression and lack of new molecular targets pose significant challenges to the effective treatment of osteosarcoma [27]. Development of individualized patient-specific treatments is severely hampered by intra- and inter-tumor heterogeneity as well as frequent and widespread structural alterations throughout the osteosarcoma genome. In fact, even patients with identical clinical conditions

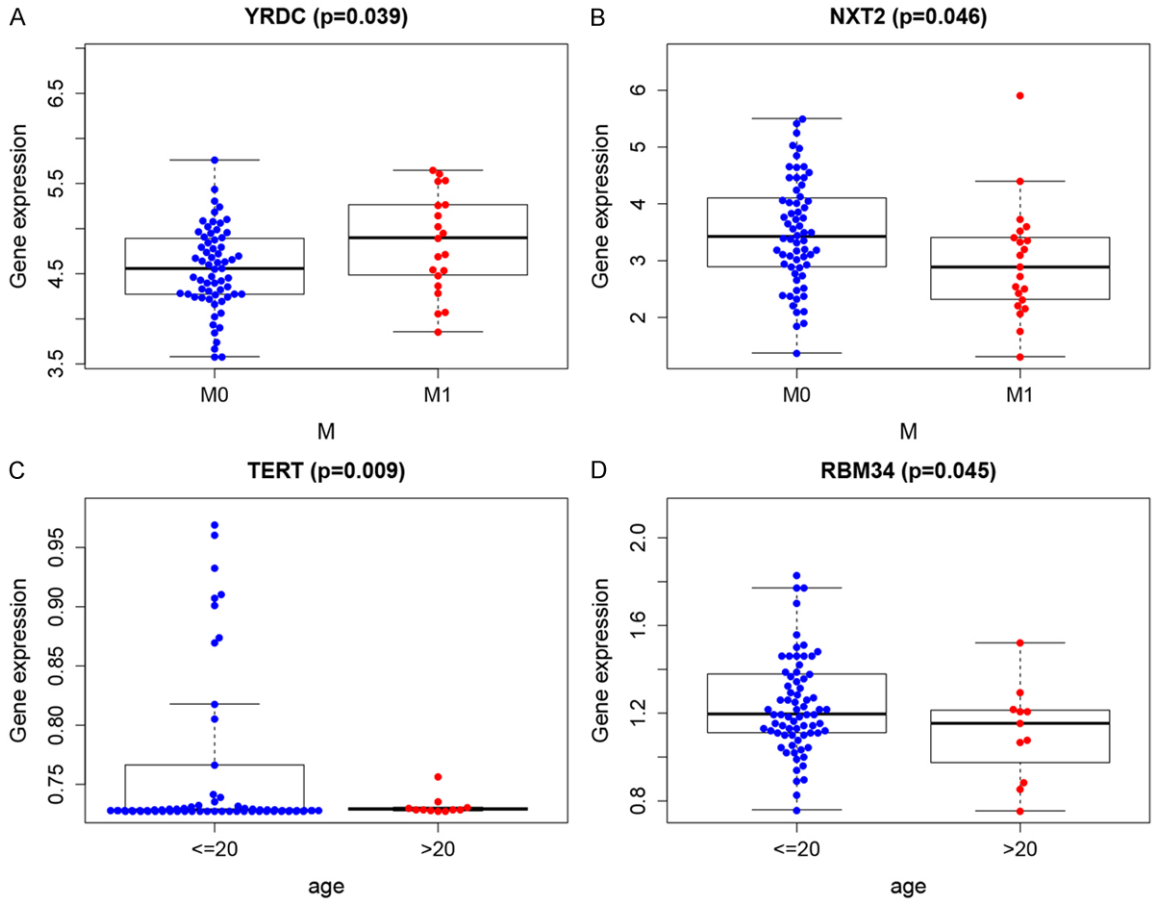

Figure 10. Clinical relevance analysis of the hub RBPs. A. Relationship between YRDC and metastasis. B. Relationship between NXT2 and metastasis. C. Relationship between TERT and age category. D. Relationship between RBM34 and age category.

often have different outcomes after receiving the same treatment [28, 29]. Hence, it is pivotal to further investigate the pathogenesis of osteosarcoma and identify new treatment targets. RNA-binding proteins (RBPs) can play a dual role in cancer development through multiple mechanisms, including mediating dysregulation of selective splicing, regulating cancer cell mRNA stability, interacting with non-coding RNAs, and modulating gene expression at the level of mRNA translation [30]. Although RBPs-related prognostic models have been reported in numerous cancers, for instance colon cancer, thyroid cancer, and gastric cancer, RBP correlation analysis in osteosarcoma has not been extensively explored [31-33]. Therefore, we constructed a RBPs-related gene signature based on transcriptomic and clinical information of osteosarcoma patients from several databases to predict survival and therapeutic response.

Herein, we screened for DERBPs in osteosarcoma tissue and control muscle tissue samples, and we found these RBPs were primarily abundant in RNA transport along with the mRNA surveillance cascade. RNA transport is an essential component of posttranscriptional regulation, and altered RNA localization can lead to cancer by promoting EMT leading to carcinogenesis [34]. For instance, several studies have demonstrated insulin-like growth factor 2 mRNA-binding proteins (IGF2BPs), a class of RBPs involved in mRNA stabilization, transport, and localization, are essential for regulating the malignant biological behavior of osteosarcoma, Ewing sarcoma, and embryonal rhabdomyosarcoma [35-39]. Among IGF2BPs, IGF2BP1 may be a prognostic biomarker for determining tumor grade, responsiveness to chemotherapy, OS, and disease-free survival in osteosarcoma patients, while dysregulation of IGF2BP3 may be associated with osteosarco-

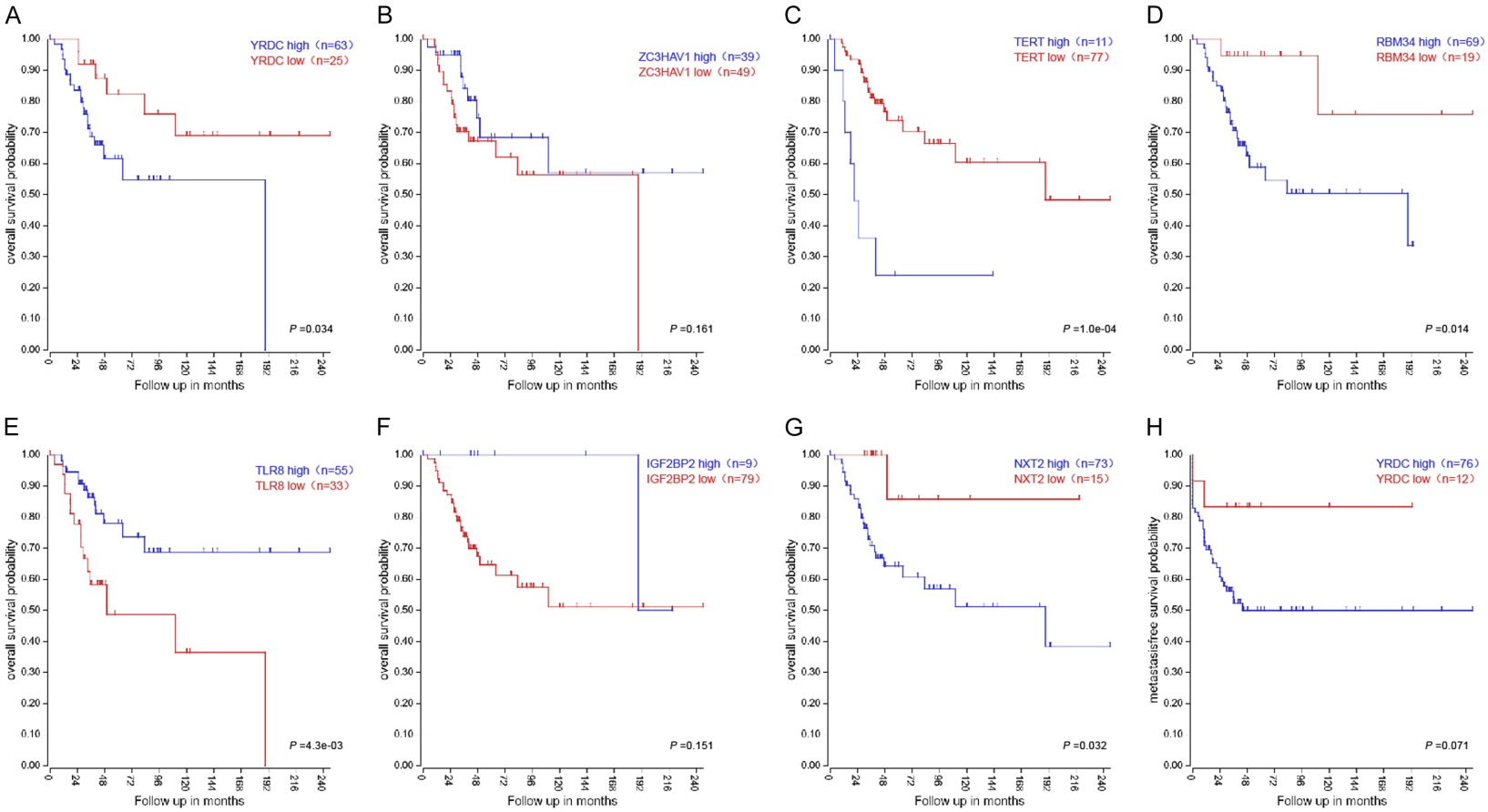
A
YRDC high (n=63)
YRDC low (n=25)
P =0.034
B
ZC3HAV1 high (n=39)
ZC3HAV1 low (n=49)
P =0.161
C
TERT high (n=11)
TERT low (n=77)
P =1.0e-04
D
RBM34 high (n=69)
RBM34 low (n=19)
P =0.014
E
TLR8 high (n=55)
TLR8 low (n=33)
P =4.3e-03
F
IGF2BP2 high (n=9)
IGF2BP2 low (n=79)
P =0.151
G
NXT2 high (n=73)
NXT2 low (n=15)
P =0.032
H
YRDC high (n=76)
YRDC low (n=12)
P =0.071
overall survival probability
metastasisfree survival probability
Follow up in months

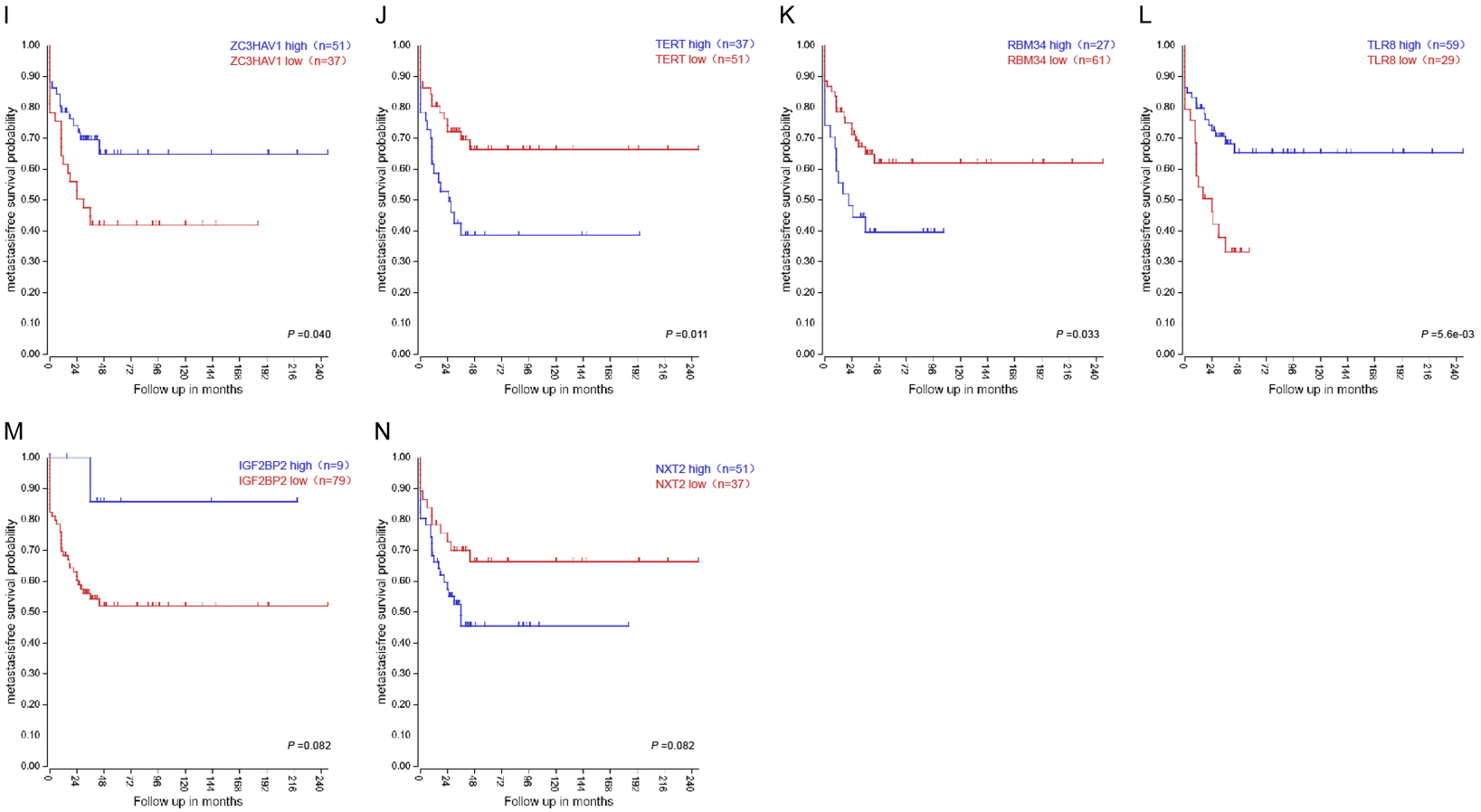

Figure 11. Prognostic value validation of seven hub RBPs. (A-G) Assessment of the association between YRDC (A), ZC3HAV1 (B), TERT (C), RBM34 (D), TLR8 (E) IGF2BP2 (F), NXT2 (G), and overall survival among osteosarcoma patients. (H-N) Analysis of the association between YRDC (H), ZC3HAV1 (I), TERT (J), RBM34 (K), TLR8 (L) IGF2BP2 (M), NXT2 (N), and metastasis-free survival among osteosarcoma patients.

Table 1. Potential small molecular drugs for patients with osteosarcoma

cmap name	mean	n	enrichment	p	specificity	percent non-null
salbutamol	-0.637	5	-0.771	0.00118	0	80
amodiaquine	-0.635	4	-0.838	0.00121	0.0066	100
prenylamine	-0.611	4	-0.825	0.00177	0.0275	100
gabapentin	-0.521	4	-0.802	0.00298	0	100
pentolonium	-0.51	5	-0.729	0.00304	0	80
lithocholic acid	-0.283	6	-0.651	0.00495	0	50

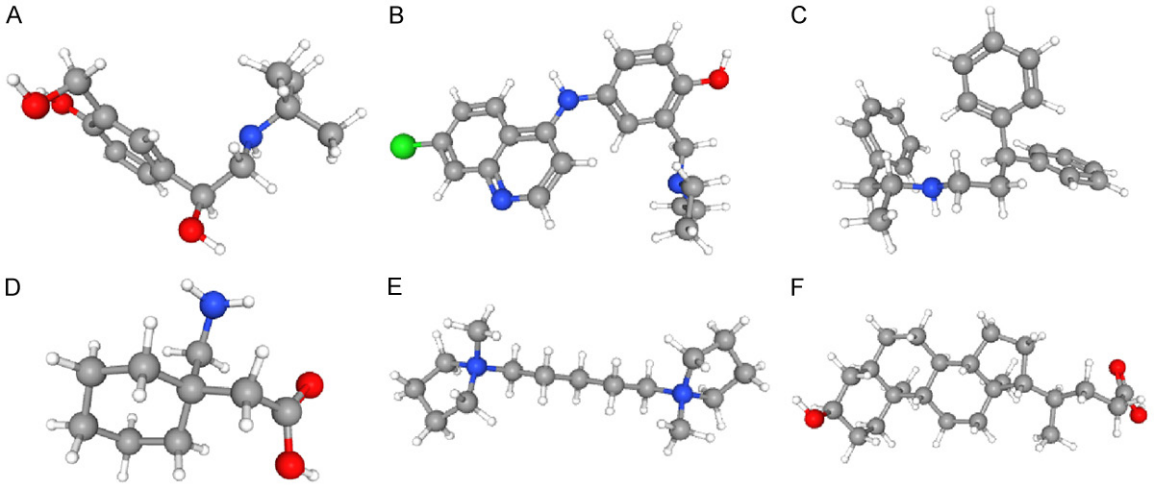

Figure 12. Six small molecule drugs for osteosarcoma. (A) Salbutamol, (B) Amodiaquine, (C) Prenylamine, (D) Gabapentin, (E) Pentoloniumand, and (F) lithocholic acid.

ma lung metastasis [40, 41]. The mRNA surveillance pathway controls the quality and quantity of mRNA to ensure the fidelity of genetic information and is also responsible for adapting cells to the tumor microenvironment [42]. RBPs are posttranscriptional regulatory molecules that perform essential RNA processing functions, including RNA maturation, selective splicing, transport, and localization [43]. In addition, RBP-mediated posttranscriptional regulation is involved in important cellular mechanisms related to carcinogenesis and tumor progression, including EMT, cell proliferation, differentiation, invasion, metastasis, apoptosis, and angiogenesis [44, 45]. Therefore, we hypothesized that RNA transport and mRNA surveillance pathway may be important mechanisms of posttranscriptional regulation by RBPs in osteosarcoma.

Considering the heterogeneity and complexity of osteosarcoma development, we conducted a deeper analysis of the RRPS. We found the RRPS has high predictive accuracy and subsequently constructed a nomogram including seven RBPs (*YRDC*, *ZC3HAV1*, *TERT*, *RBM34*, *TLR8*, *IGF2BP2*, and *NXT2*) to predict one-, three-, and five-year survival rates in osteosarcoma patients to guide clinical decision making. Numerous studies have shown *YRDC* is involved in regulating telomere length, N6-threonylcarbamoyladenosine biosynthesis of tRNA, and protein translation quality [46]. Hu et al. also reported that high *YRDC* expression promoted the growth of colon adenocarcinoma cells, but interestingly, high *YRDC* expression was also associated with a better prognosis [47]. In hepatocellular carcinoma, *YRDC* promoted Huh7 cell proliferation, migration, and invasion by activating the MEK/ERK signaling pathway, and was associated with resistance to lenvatinib [48]. However, the roles of *YRDC* in osteosarcoma and related mechanisms have not been reported. *ZC3HAV1* has been associated with the anti-Sindbis virus (SINV) ability of U2OS cells, and *ZC3HAV1* overexpression reduced SINV replication by more than 10-fold [49]. In addition, *ZC3HAV1* expression was neg-

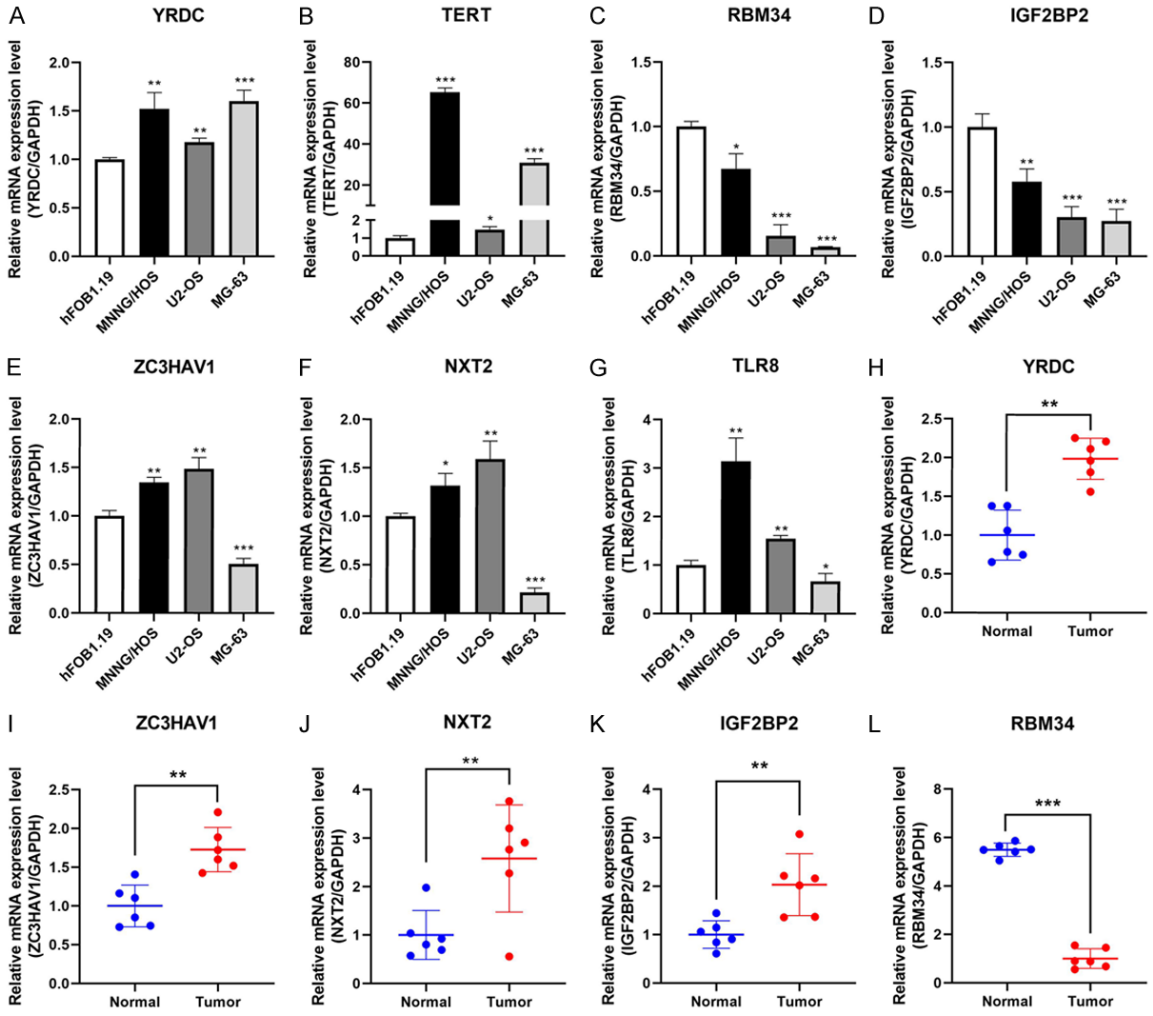

Figure 13. Expression validation of seven hub RBP genes. (A-G) The expression of *YRDC* (A), *TERT* (B), *RBM34* (C), *IGF2BP2* (D), *ZC3HAV1* (E), *NXT2* (F), and *TLR8* (G) in the osteosarcoma cells compared to osteoblasts. (H-L) The expression of *YRDC* (H), *ZC3HAV1* (I), *NXT2* (J), *IGF2BP2* (K), and RBM34 (L) in osteosarcoma tissues compared to normal tissues (*P < 0.05, **P < 0.01 and ***P < 0.001).

atively associated with the yield of Human T cell leukaemia virus type 1 virus, and ZC3HAV1-mediated inhibition was also observed in other delta-type retroviruses [50]. However, the role of *ZC3HAV1* in cancer has not been studied extensively. The current study has shown ZC3HAV1 upregulates expression of EMT-related markers, cyclin D1 and CDK2, and binds directly to KRAS to promote proliferation and metastasis of pancreatic cancer [51]. TERT plays a key role in the regulation of aging and cancer development by reactivating telomerase, which maintains telomere length and promotes alternative lengthening of telomeres [52]. In another study, Sanders et al. reported high *TERT* expression in osteosarcoma patients was associated with poor OS and PFS [53]. In contrast, knockdown of TERT inhibited osteosarcoma proliferation by decreasing telomerase activity along with increasing levels of apoptosis-related proteins [54]. Notably, TERT also plays an important role in cisplatin resistance in osteosarcoma by inhibiting apoptosis through the mitochondrial pathway or by attenuating intracellular reactive oxygen species [55]. Consistent with the above studies, our study showed *TERT* was highly expressed in osteosarcoma and was associated with poor prognosis. *RBM34* contains an RNA recognition sequence, which is mainly involved in mRNA processing [56]. According to our analysis, osteosarcoma patients with high *RBM34*

expression had worse OS and MFS, which suggests *RBM34* may promote osteosarcoma progression. TLR8, a pattern recognition receptor, is a critical component responsible for triggering the innate immune response and is a relevant therapeutic target for cancer [57]. Notably, TLR8 agonists used in combination with ICI demonstrated powerful synergistic effects and can improve the prognosis of cancer patients [58]. In another study, Adepoju et al. observed that polyuridylic acid induced apoptosis and inhibited tumor cell proliferation in osteosarcoma cells, and this effect was partly associated with TLR8 [59]. In addition, *TLR8* expression helps to identify immune infiltrating cell subpopulations and tumor purity in triple-negative breast cancer, which further illustrates the potential of TLR8 in tumor immunotherapy [60]. IGF2BP2 is both an N6-methyladenosine regulator and an RNA-binding protein, which is aberrantly expressed in a variety of cancers and associated with prognosis [61]. In a study by Chen et al., lncRNA human leukocyte antigen complex group 11 could stabilize p27 Kip1 mRNA by binding to IGF2BP2 thereby inhibiting osteosarcoma proliferation [62]. Notably, another study showed that IGF2BP2 was lowly expressed in MNNG/HOS and MG-63 cell lines, which is consistent with our findings [63]. However, IGF2BP2 was overexpressed in osteosarcoma tissues relative to control tissues, which may be a function of the different tumor growth environment in vitro and in vivo, and additional investigation is needed to elucidate the specific reasons for this. NXT2 is involved in mRNA and protein export and may play a role in early spermatogenesis [64, 65]. Malone et al. also detected *NXT2* expression in drug-resistant neuroblastoma cell lines and proposed selective regulation of the essential protein NXF1 for cancer treatment by exploiting the NXT1-NXT2 paralog relationship. However, the mechanism of action of NXT2 in other cancers has not been fully elucidated [66]. In the present study we examined the contents of the seven key RBPs mentioned above in osteosarcoma relative to osteoblasts, hoping to provide a foundation for further ex vivo studies.

Furthermore, we compared the degree of immune cell infiltration as well as immune pathway activity in osteosarcoma patients with high and low RRPS-scores and examined the distribution of immune scores, and tumor purity along with stromal scores in individuals with osteosarcoma. We found that the low RRPS-score group showed higher immune scores, stromal scores, immune cell infiltration, and immune functions. Consistent with the above data, the high-scoring group exhibited high tumor purity. Unsurprisingly, our results also showed worse OS in the high-scoring group relative to the low-scoring group. We speculate suppression of both intrinsic and adaptive immunity may contribute to the worse prognosis among osteosarcoma patients in the high-scoring group. In summary, the RRPS can assess immune microenvironment features, which may help guide antitumor treatment strategies. ICI treatment is a superior immunotherapeutic approach that blocks the immune checkpoint signaling pathway and enhances T-cell immune response, which allows for rapid and durable treatment of patients with cancer, especially those with advanced solid tumors [69]. Despite its benefits, ICI therapy has a major drawback - only some patients respond to it [70]. Therefore, individualized treatment, based on characteristics such as tumor specificity and patient clinicopathologic factors, is needed to select patients most likely to respond to ICI therapy. In our study, patients with high RRPS-scores had low expression of immune checkpoint genes. Therefore, the RRPS may be useful to assess whether patients can benefit from ICI therapy. In addition, we screened potential small molecule drugs that may be helpful in improving the prognosis of osteosarcoma patients.

There are some inevitable limitations of our study. First, we recognize that further tumor histological verification at the individual level as well as in vivo experiments using animal models may better reveal the specific roles and mechanisms of the seven key RBPs in osteosarcoma. However, in this study, we mainly focused on constructing an RBP-based signature and exploring its potential to identify patients that may be candidates for immunotherapy. Therefore, more studies are needed to validate our research. In addition, the inherent limitation of insufficient sample size in the clinical databases necessitates further osteosarcoma samples collection to validate the accuracy of the model. It is also necessary to test the effectiveness of the screened drugs in the treatment of osteosarcoma.

Conclusion

We designed and verified a reliable signature comprised of seven RBPs for osteosarcoma, which is pivotal in early diagnosis and prediction of response to immunotherapy.

Acknowledgements

This work was supported by the National Natural Science Foundation of China (No. 81601931; 81672229), the Natural Science Foundation of Jiangsu Province (BK20150475), the Youth Medical Key Talent Project of Jiangsu (QNRC2016844), "Six One Projects" for high-level health professionals in Jiangsu Province Top Talent Project (LGY2019089), Jiangsu Provincial key research and development program (BE2020679), Medical Education Collaborative Innovation Fund Of Jiangsu University (JDY2022001), Jiangsu Province Postgraduate Practice Innovation Program (No. SJCX20_1434), and the Shenzhen Science and Technology Program (No. KQTD201708101540-11370).

Disclosure of conflict of interest

None.

Address correspondence to: Yiming Zhang, Department of Orthopedics, Affiliated Hospital of Jiangsu University, Zhenjiang 212001, Jiangsu, China. E-mail: zhangyiming0607@163.com; Qiping Zheng, Department of Laboratory Science, School of Medicine, Jiangsu University, Zhenjiang 212013, Jiangsu, China. E-mail: qp_zheng@hotmail.com

References

[1] Rojas GA, Hubbard AK, Diessner BJ, Ribeiro KB and Spector LG. International trends in incidence of osteosarcoma (1988-2012). Int J Cancer 2021; 149: 1044-1053.

[2] Zhou J, Wang M, Zhou Z, Wang W, Duan J and Wu G. Expression and prognostic value of MCM family genes in osteosarcoma. Front Mol Biosci 2021; 8: 668402.

[3] Zhang XR, Shao JL, Li H and Wang L. Silencing of LINC00707 suppresses cell proliferation, migration, and invasion of osteosarcoma cells by modulating miR-338-3p/AHSA1 axis. Open Life Sci 2021; 16: 728-736.

[4] Xie X, Xiao Y and Huang X. Homeobox C10 knockdown suppresses cell proliferation and promotes cell apoptosis in osteosarcoma cells through regulating caspase 3. Onco Targets Ther 2018; 11: 473-482.

[5] Papakonstantinou E, Stamatopoulos A, D IA, Kenanidis E, Potoupnis M, Haidich AB and Tsiridis E. Limb-salvage surgery offers better five-year survival rate than amputation in patients with limb osteosarcoma treated with neoadjuvant chemotherapy. A systematic review and meta-analysis. J Bone Oncol 2020; 25: 100319.

[6] Miao Y, Liu G and Liu L. Histone methyltransferase SUV39H2 regulates LSD1-dependent CDH1 expression and promotes epithelial mesenchymal transition of osteosarcoma. Cancer Cell Int 2021; 21: 2.

[7] Yao Q and Chen T. LINC01128 regulates the development of osteosarcoma by sponging miR-299-3p to mediate MMP2 expression and activating Wnt/β-catenin signalling pathway. J Cell Mol Med 2020; 24: 14293-14305.

[8] Fan Z, Huang G, Zhao J, Li W, Lin T, Su Q, Yin J and Shen J. Establishment and characterization of a highly metastatic human osteosarcoma cell line from osteosarcoma lung metastases. J Bone Oncol 2021; 29: 100378.

[9] Ren HY, Sun LL, Li HY and Ye ZM. Prognostic significance of serum alkaline phosphatase level in osteosarcoma: a meta-analysis of published data. Biomed Res Int 2015; 2015: 160835.

[10] Corre I, Verrecchia F, Crenn V, Redini F and Trichet V. The osteosarcoma microenvironment: a complex but targetable ecosystem. Cells 2020; 9: 976.

[11] Zhang J, Dai Z, Yan C, Zhang W, Wang D and Tang D. A new biological triangle in cancer: intestinal microbiota, immune checkpoint inhibitors and antibiotics. Clin Transl Oncol 2021; 23: 2415-2430.

[12] Hosseinzadeh R, Feizisani F, Shomali N, Abdelbasset WK, Hemmatzadeh M, Gholizadeh Navashenaq J, Jadidi-Niaragh F, Bokov DO, Janebifam M and Mohammadi H. PD-1/PD-L1 blockade: prospectives for immunotherapy in cancer and autoimmunity. IUBMB Life 2021; 73: 1293-1306.

[13] Zhang Y, He R, Lei X, Mao L, Jiang P, Ni C, Yin Z, Zhong X, Chen C, Zheng Q and Li D. A novel pyroptosis-related signature for predicting prognosis and indicating immune microenvironment features in osteosarcoma. Front Genet 2021; 12: 780780.

[14] Zheng D, Yang K, Chen X, Li Y and Chen Y. Analysis of immune-stromal score-based gene signature and molecular subtypes in osteosarcoma: implications for prognosis and tumor immune microenvironment. Front Genet 2021; 12: 699385.

[15] Gerstberger S, Hafner M and Tuschl T. A census of human RNA-binding proteins. Nat Rev Genet 2014; 15: 829-845.

[16] Mohibi S, Chen X and Zhang J. Cancer the 'RBP' eutics-RNA-binding proteins as thera-

peutic targets for cancer. Pharmacol Ther 2019; 203: 107390.
[17] Pereira B, Billaud M and Almeida R. RNA-binding proteins in cancer: old players and new actors. Trends Cancer 2017; 3: 506-528.
[18] Bell JL, Wächter K, Mühleck B, Pazaitis N, Köhn M, Lederer M and Hüttelmaier S. Insulin-like growth factor 2 mRNA-binding proteins (IGF2BPs): post-transcriptional drivers of cancer progression? Cell Mol Life Sci 2013; 70: 2657.
[19] Huang X, Zhang H, Guo X, Zhu Z, Cai H and Kong X. Insulin-like growth factor 2 mRNA-binding protein 1 (IGF2BP1) in cancer. J Hematol Oncol 2018; 11: 88.
[20] Wang H, Ding N, Guo J, Xia J and Ruan Y. Dysregulation of TTP and HuR plays an important role in cancers. Tumour Biol 2016; 37: 14451-14461.
[21] Guo Q, Wu Y, Guo X, Cao L, Xu F, Zhao H, Zhu J, Wen H, Ju X and Wu X. The RNA-Binding protein CELF2 inhibits ovarian cancer progression by stabilizing FAM198B. Mol Ther Nucleic Acids 2021; 23: 169-184.
[22] Wu ZL, Deng YJ, Zhang GZ, Ren EH, Yuan WH and Xie QQ. Development of a novel immune-related genes prognostic signature for osteosarcoma. Sci Rep 2020; 10: 18402.
[23] Zhang J, Ding R, Wu T, Jia J and Cheng X. Autophagy-related genes and long noncoding RNAs signatures as predictive biomarkers for osteosarcoma survival. Front Cell Dev Biol 2021; 9: 705291.
[24] Chen Z, Wu H, Yang H, Fan Y, Zhao S and Zhang M. Identification and validation of RNA-binding protein-related gene signature revealed potential associations with immunosuppression and drug sensitivity in glioma. Cancer Med 2021; 10: 7418-7439.
[25] Otoukesh B, Boddouhi B, Moghtadaei M, Kaghazian P and Kaghazian M. Novel molecular insights and new therapeutic strategies in osteosarcoma. Cancer Cell Int 2018; 18: 158.
[26] Chong ZX, Yeap SK and Ho WY. Unraveling the roles of miRNAs in regulating epithelial-to-mesenchymal transition (EMT) in osteosarcoma. Pharmacol Res 2021; 172: 105818.
[27] Zheng D, Xia K, Yu L, Gong C, Shi Y, Li W, Qiu Y, Yang J and Guo W. A novel six metastasis-related prognostic gene signature for patients with osteosarcoma. Front Cell Dev Biol 2021; 9: 699212.
[28] Landuzzi L, Manara MC, Lollini PL and Scotlandi K. Patient derived xenografts for genome-driven therapy of osteosarcoma. Cells 2021; 10: 416.
[29] Schott C, Shah AT and Sweet-Cordero EA. Genomic complexity of osteosarcoma and its implication for preclinical and clinical targeted therapies. Adv Exp Med Biol 2020; 1258: 1-19.
[30] Bitaraf A, Razmara E, Bakhshinejad B, Yousefi H, Vatanmakanian M, Garshasbi M, Cho WC and Babashah S. The oncogenic and tumor suppressive roles of RNA-binding proteins in human cancers. J Cell Physiol 2021; 236: 6200-6224.
[31] Chang K, Yuan C and Liu X. A new RBPs-related signature predicts the prognosis of colon adenocarcinoma patients. Front Oncol 2021; 11: 627504.
[32] Ma Y, Yin S, Liu XF, Hu J, Cai N, Zhang XB, Fu L, Cao XC and Yu Y. Comprehensive analysis of the functions and prognostic value of RNA-binding proteins in thyroid cancer. Front Oncol 2021; 11: 625007.
[33] Qiu Z, Jiang H, Ju K and Liu X. A novel RNA-binding protein signature to predict clinical outcomes and guide clinical therapy in gastric cancer. Front Med (Lausanne) 2021; 8: 670141.
[34] Engel KL, Arora A, Goering R, Lo HG and Taliaferro JM. Mechanisms and consequences of subcellular RNA localization across diverse cell types. Traffic 2020; 21: 404-418.
[35] Korn SM, Ulshöfer CJ, Schneider T and Schlundt A. Structures and target RNA preferences of the RNA-binding protein family of IGF2BPs: an overview. Structure 2021; 29: 787-803.
[36] Li Z, Zhang Y, Ramanujan K, Ma Y, Kirsch DG and Glass DJ. Oncogenic NRAS, required for pathogenesis of embryonic rhabdomyosarcoma, relies upon the HMGA2-IGF2BP2 pathway. Cancer Res 2013; 73: 3041-3050.
[37] Chen W, Chen M, Xu Y, Chen X, Zhou P, Zhao X, Pang F and Liang W. Long non-coding RNA THOR promotes human osteosarcoma cell growth in vitro and in vivo. Biochem Biophys Res Commun 2018; 499: 913-919.
[38] Mancarella C, Pasello M, Ventura S, Grilli A, Calzolari L, Toracchio L, Lollini PL, Donati DM, Picci P, Ferrari S and Scotlandi K. Insulin-like growth factor 2 mRNA-binding protein 3 is a novel post-transcriptional regulator of ewing sarcoma malignancy. Clin Cancer Res 2018; 24: 3704-3716.
[39] Rivera Vargas T, Boudoukha S, Simon A, Souidi M, Cuvellier S, Pinna G and Polesskaya A. Post-transcriptional regulation of cyclins D1, D3 and G1 and proliferation of human cancer cells depend on IMP-3 nuclear localization. Oncogene 2014; 33: 2866-2875.
[40] Heng L, Jia Z, Bai J, Zhang K, Zhu Y, Ma J, Zhang J and Duan H. Molecular characterization of metastatic osteosarcoma: differentially expressed genes, transcription factors and microRNAs. Mol Med Rep 2017; 15: 2829-2836.

[41] Wang L, Aireti A, Aihaiti A and Li K. Expression of microRNA-150 and its target gene IGF2BP1 in human osteosarcoma and their clinical implications. Pathol Oncol Res 2019; 25: 527-533.
[42] Popp MW and Maquat LE. Nonsense-mediated mRNA decay and cancer. Curr Opin Genet Dev 2018; 48: 44-50.
[43] Zhang B, Babu KR, Lim CY, Kwok ZH, Li J, Zhou S, Yang H and Tay Y. A comprehensive expression landscape of RNA-binding proteins (RBPs) across 16 human cancer types. RNA Biol 2020; 17: 211-226.
[44] Neelamraju Y, Gonzalez-Perez A, Bhat-Nakshatri P, Nakshatri H and Janga SC. Mutational landscape of RNA-binding proteins in human cancers. RNA Biol 2018; 15: 115-129.
[45] Kang D, Lee Y and Lee JS. RNA-binding proteins in cancer: functional and therapeutic perspectives. Cancers (Basel) 2020; 12: 2699.
[46] Huang S, Zhu P, Sun B, Guo J, Zhou H, Shu Y and Li Q. Modulation of YrdC promotes hepatocellular carcinoma progression via MEK/ERK signaling pathway. Biomed Pharmacother 2019; 114: 108859.
[47] Hu M, Fu X, Si Z, Li C, Sun J, Du X and Zhang H. Identification of differently expressed genes associated with prognosis and growth in colon adenocarcinoma based on integrated bioinformatics analysis. Front Genet 2019; 10: 1245.
[48] Guo J, Zhu P, Ye Z, Wang M, Yang H, Huang S, Shu Y, Zhang W, Zhou H and Li Q. YRDC mediates the resistance of lenvatinib in hepatocarcinoma cells via modulating the translation of KRAS. Front Pharmacol 2021; 12: 744578.
[49] Law LMJ, Razooky BS, Li MMH, You S, Jurado A, Rice CM and MacDonald MR. ZAP's stress granule localization is correlated with its antiviral activity and induced by virus replication. PLoS Pathog 2019; 15: e1007798.
[50] Miyazato P, Matsuo M, Tan BJY, Tokunaga M, Katsuya H, Islam S, Ito J, Murakawa Y and Satou Y. HTLV-1 contains a high CG dinucleotide content and is susceptible to the host antiviral protein ZAP. Retrovirology 2019; 16: 38.
[51] Huang W, Hua H, Xiao G, Yang X, Yang Q and Jin L. ZC3HAV1 promotes the proliferation and metastasis via regulating KRAS in pancreatic cancer. Aging (Albany NY) 2021; 13: 18482-18497.
[52] Dratwa M, Wysoczańska B, Łacina P, Kubik T and Bogunia-Kubik K. TERT-regulation and roles in cancer formation. Front Immunol 2020; 11: 589929.
[53] Sanders RP, Drissi R, Billups CA, Daw NC, Valentine MB and Dome JS. Telomerase expression predicts unfavorable outcome in osteosarcoma. J Clin Oncol 2004; 22: 3790-3797.
[54] Chen P, Gu WL, Gong MZ, Wang J and Li DQ. shRNA-mediated silencing of hTERT suppresses proliferation and promotes apoptosis in osteosarcoma cells. Cancer Gene Ther 2017; 24: 325-332.
[55] Zhang Z, Yu L, Dai G, Xia K, Liu G, Song Q, Tao C, Gao T and Guo W. Telomerase reverse transcriptase promotes chemoresistance by suppressing cisplatin-dependent apoptosis in osteosarcoma cells. Sci Rep 2017; 7: 7070.
[56] Kim JY, Kim YG and Lee GM. Differential in-gel electrophoresis (DIGE) analysis of CHO cells under hyperosmotic pressure: osmoprotective effect of glycine betaine addition. Biotechnol Bioeng 2012; 109: 1395-1403.
[57] Talukdar A, Ganguly D, Roy S, Das N and Sarkar D. Structural evolution and translational potential for agonists and antagonists of endosomal toll-like receptors. J Med Chem 2021; 64: 8010-8041.
[58] Varshney D, Qiu SY, Graf TP and McHugh KJ. Employing drug delivery strategies to overcome challenges using TLR7/8 agonists for cancer immunotherapy. AAPS J 2021; 23: 90.
[59] Adepoju LJ and Geiger JD. Antitumor activity of polyuridylic acid in human soft tissue and bone sarcomas. J Surg Res 2010; 164: e107-114.
[60] Roychowdhury A, Jondhale M, Saldanha E, Ghosh D, Kumar Panda C, Chandrani P and Mukherjee N. Landscape of toll-like receptors expression in tumor microenvironment of triple negative breast cancer (TNBC): distinct roles of TLR4 and TLR8. Gene 2021; 792: 145728.
[61] Wang J, Chen L and Qiang P. The role of IGF2BP2, an m6A reader gene, in human metabolic diseases and cancers. Cancer Cell Int 2021; 21: 99.
[62] Gu J, Dai B, Shi X, He Z, Xu Y, Meng X and Zhu J. lncRNA HCG11 suppresses human osteosarcoma growth through upregulating p27 Kip1. Aging (Albany NY) 2021; 13: 21743-21757.
[63] Li B, Fang L, Wang B, Yang Z and Zhao T. Identification of prognostic RBPs in osteosarcoma. Technol Cancer Res Treat 2021; 20: 15330338211004918.
[64] Khan M, Jabeen N, Khan T, Hussain HMJ, Ali A, Khan R, Jiang L, Li T, Tao Q, Zhang X, Yin H, Yu C, Jiang X and Shi Q. The evolutionarily conserved genes: Tex37, Ccdc73, Prss55 and Nxt2 are dispensable for fertility in mice. Sci Rep 2018; 8: 4975.
[65] Zadel M, Maver A, Kovanda A and Peterlin B. DNA methylation profiles in whole blood of huntington's disease patients. Front Neurol 2018; 9: 655.
[66] Malone CF, Dharia NV, Kugener G, Forman AB, Rothberg MV, Abdusamad M, Gonzalez A, Kuljanin M, Robichaud AL, Conway AS, Dempster JM, Paolella BR, Dumont N, Hovestadt V, Mancias JD, Younger ST, Root DE, Golub TR,

Vazquez F and Stegmaier K. Selective modulation of a pan-essential protein as a therapeutic strategy in cancer. Cancer Discov 2021; 11: 2282-2299.

[67] Ma LR, Li JX, Tang L, Li RZ, Yang JS, Sun A, Leung EL and Yan PY. Immune checkpoints and immunotherapy in non-small cell lung cancer: novel study progression, challenges and solutions. Oncol Lett 2021; 22: 787.

[68] Titov A, Zmievskaya E, Ganeeva I, Valiullina A, Petukhov A, Rakhmatullina A, Miftakhova R, Fainshtein M, Rizvanov A and Bulatov E. Adoptive immunotherapy beyond CAR T-cells. Cancers (Basel) 2021; 13: 743.

[69] Larroquette M, Domblides C, Lefort F, Lasserre M, Quivy A, Sionneau B, Bertolaso P, Gross-Goupil M, Ravaud A and Daste A. Combining immune checkpoint inhibitors with chemotherapy in advanced solid tumours: a review. Eur J Cancer 2021; 158: 47-62.

[70] Kraehenbuehl L, Weng CH, Eghbali S, Wolchok JD and Merghoub T. Enhancing immunotherapy in cancer by targeting emerging immunomodulatory pathways. Nat Rev Clin Oncol 2022; 19: 37-50.

Supplementary Table 2. Primers for qRT-PCR

Primer	Direction	Sequence (5'-3')
YRDC	Forward	CTAAACCCTTTTACGCCTCTTGT
	Reverse	CGGACCCTCAAACATCTGAGC
ZC3HAV1	Forward	TCACGAACTCTCTGGACTGAA
	Reverse	ACTTTTGCATATCTCGGGCATAA
TERT	Forward	TCACGGAGACCACGTTTCAAA
	Reverse	TTCAAGTGCTGTCTGATTCCAAT
RBM34	Forward	ATGGCCTTGGAAGGGATGAG
	Reverse	GAACGCCGTCGTCAGGATT
TLR8	Forward	AACTGCCAAGCTCCCTACG
	Reverse	CAAGGCACGCATGGAAATGG
IGF2BP2	Forward	AGCTAAGCGGGCATCAGTTTG
	Reverse	CCGCAGCGGGAAATCAATCT
NXT2	Forward	GGACAAGGCCACCTTAATATGG
	Reverse	TGGAACTCACTAGAAGGCAATGT

Supplementary Table 3. Identification of DERBPs in osteosarcoma and normal tissues

gene	conMean	treatMean	logFC	*p*Value	fdr
PSMA6	6.687632091	3.302836548	-1.017789907	8.33E-49	1.58E-47
TRIM56	1.733127403	4.008248584	1.209594273	2.89E-48	2.80E-47
TRIM71	0.006713723	0.292928076	5.447289616	1.45E-39	4.32E-39
FDXACB1	0.305687801	0.75710797	1.308440072	4.19E-37	1.09E-36
MSI1	0.079262709	1.402921767	4.145648469	1.84E-40	5.71E-40
MSI2	4.150985559	1.708572443	-1.280662494	9.15E-48	6.83E-47
RBMS2	1.603258504	3.428223901	1.096454277	1.25E-46	7.24E-46
RBFOX1	5.022459151	0.110109647	-5.511381147	1.40E-48	1.80E-47
RBFOX3	0.316906397	0.101354827	-1.644641983	3.74E-36	9.32E-36
CWF19L2	1.801614342	3.773629368	1.066662517	6.26E-44	2.46E-43
L1TD1	0.032704752	0.114203445	1.804033976	2.49E-11	3.37E-11
SRSF12	0.252789779	0.756371429	1.581156735	2.17E-26	4.00E-26
TOE1	1.259511187	3.033489911	1.268114577	3.16E-48	2.95E-47
STAU2	4.620390324	2.257453608	-1.033318394	4.15E-47	2.67E-46
ELAVL4	0.036326626	0.140735125	1.953883152	8.22E-20	1.31E-19
RBM43	0.676340474	2.012823023	1.573398733	1.27E-43	4.85E-43
TOP3B	2.477877554	0.189792946	-3.706606618	8.47E-49	1.58E-47
NCBP2L	0.09745337	0.027130587	-1.844791818	4.36E-20	6.97E-20
TDRD9	0.255328817	0.789478568	1.628543727	0.006130504	0.006826502
ZC3H12B	0.152987661	0.414488549	1.437916944	1.34E-22	2.27E-22
ZC3H12D	0.164832189	0.388271951	1.236069489	6.73E-25	1.20E-24
PABPN1L	0.05752597	0.021338804	-1.430734052	6.36E-12	8.71E-12
EEF1G	9.871388925	0.297677215	-5.051432385	7.33E-49	1.58E-47
RPP25	0.616337221	3.399683388	2.463608569	4.78E-48	4.00E-47
RDM1	0.015573634	0.28752918	4.206530883	4.06E-36	1.01E-35
DZIP1	1.03586749	2.628347156	1.343316379	6.84E-43	2.44E-42
HBS1L	5.151434303	2.232661598	-1.206209574	1.13E-48	1.59E-47
DARS2	1.604053141	3.804212929	1.245876061	6.28E-48	4.94E-47
GTPBP10	2.688231127	1.326495925	-1.019036939	4.18E-45	1.92E-44
HENMT1	0.923394773	3.547964602	1.941972145	3.37E-46	1.79E-45

RNASEK	6.674160536	3.084436543	-1.113579423	8.17E-49	1.58E-47
IPO4	3.565463753	1.256841417	-1.504287109	7.85E-48	5.98E-47
MRPL38	5.41164792	2.141837918	-1.337218671	8.45E-49	1.58E-47
APOBEC2	6.689418856	0.698185698	-3.260198172	1.23E-47	8.92E-47
APOBEC3H	0.084707891	0.237203935	1.485559675	1.47E-05	1.75E-05
APOBEC3F	0.272642412	1.42073454	2.381555109	2.35E-47	1.58E-46
APOBEC3G	0.581127283	1.42447096	1.293500115	4.99E-31	1.05E-30
EIF5A2	0.534101397	1.546890085	1.534185127	4.88E-44	1.94E-43
EIF5AL1	0.501165298	1.36897235	1.44973488	4.15E-36	1.03E-35
BOLL	0.943372706	0.044142677	-4.417581823	3.25E-47	2.13E-46
DAZL	0.01299315	0.177102323	3.768759984	1.07E-25	1.95E-25
FBXO17	1.261037093	3.324557704	1.398551706	2.11E-43	7.87E-43
ZC3HAV1	1.021791681	4.169194535	2.028667595	8.86E-49	1.58E-47
POLR2J2	0.705564656	0.033447028	-4.39882837	2.22E-47	1.52E-46
POLR2J3	4.978639131	0.989553173	-2.330902311	8.48E-49	1.58E-47
ZCCHC2	3.449058165	1.314642339	-1.391532105	3.66E-48	3.29E-47
PTRH1	2.745799441	0.096928332	-4.824164018	8.48E-49	1.58E-47
AZGP1	0.707313688	0.046950484	-3.913138256	5.32E-45	2.37E-44
NYNRIN	0.79628083	2.509434418	1.656013012	1.18E-38	3.34E-38
RBM44	0.287859541	0.125875839	-1.193363636	1.64E-26	3.03E-26
OASL	0.216730872	2.044838847	3.238010575	2.01E-43	7.54E-43
OAS1	0.888817137	2.483980044	1.482695045	7.41E-32	1.59E-31
OAS2	0.84421719	3.258239425	1.948406511	1.50E-42	5.18E-42
OAS3	0.794321218	3.398455774	2.097084903	4.39E-44	1.75E-43
MBNL3	0.352263965	1.094835519	1.63598534	6.91E-39	1.99E-38
PUS7L	0.726668099	1.562296032	1.104299371	1.58E-44	6.64E-44
MRPS24	6.779676768	3.129099877	-1.115468784	8.29E-49	1.58E-47
RPS27L	5.782304534	2.572010795	-1.168747895	1.01E-48	1.58E-47
SMAD2	3.869385168	1.725417633	-1.165158741	8.48E-49	1.58E-47
SMAD6	0.84882896	3.600676341	2.08472214	4.83E-46	2.50E-45
ADARB2	0.138180155	0.046299212	-1.577490907	1.31E-10	1.75E-10
ADAD2	0.246250838	0.042689261	-2.528183522	4.61E-27	8.66E-27
CLK3	4.722043167	1.830177882	-1.367427354	8.47E-49	1.58E-47
CLK4	3.991806628	1.292201778	-1.62721047	8.48E-49	1.58E-47
EIF4A1	6.595619646	2.082812695	-1.662975099	8.43E-49	1.58E-47
IGF2BP1	0.02000366	1.38887262	6.117506472	1.66E-44	6.97E-44
IGF2BP2	0.843391641	3.058303362	1.858456891	3.49E-26	6.39E-26
IGF2BP3	0.051242006	1.555166596	4.923598373	8.55E-48	6.44E-47
NSUN7	0.090371574	0.515656193	2.512468528	1.32E-28	2.56E-28
TDRD10	1.012299745	0.352313158	-1.522706279	2.21E-38	6.17E-38
ENDOV	2.925295109	1.450252575	-1.012277993	1.15E-43	4.41E-43
MRRF	4.102160455	1.383660381	-1.567894046	8.47E-49	1.58E-47
PSTK	1.468145779	0.719152811	-1.029624964	2.74E-34	6.35E-34
MOV10L1	0.054058825	0.111856987	1.049053322	6.71E-06	8.08E-06
AFF2	0.050512602	0.717526499	3.828316861	3.26E-40	9.96E-40
SRBD1	1.116040757	2.692370667	1.27048733	1.93E-48	2.14E-47
MATR3	4.551097157	0.477517289	-3.252589512	8.46E-49	1.58E-47
RBM46	0.007851073	0.094771693	3.593494545	2.73E-06	3.31E-06
RBM47	0.276015665	1.377050383	2.318759292	6.72E-42	2.26E-41

DND1	0.340475901	0.001589081	-7.743216287	2.10E-48	2.25E-47
RBM20	2.407919374	0.663317515	-1.86001556	2.04E-43	7.65E-43
GNL3L	1.730856933	4.774267254	1.463792847	9.89E-49	1.58E-47
KHDC1	0.414583923	1.214082938	1.550130904	3.19E-38	8.77E-38
KHDC1L	0.02065645	0.093612684	2.180111663	1.17E-09	1.52E-09
RPL10L	0.017297494	0.349174031	4.335311342	1.03E-41	3.43E-41
IFIH1	0.695416705	2.309558416	1.731667409	8.31E-41	2.62E-40
RNF113B	0.016046702	0.092240923	2.523130109	7.88E-07	9.68E-07
LENG9	0.823212384	1.857625675	1.174123227	1.24E-29	2.49E-29
RPS29	9.99495031	4.51373199	-1.146878636	5.09E-49	1.58E-47
U2AF1	4.513232001	0.357910738	-3.656489209	8.47E-49	1.58E-47
U2AF1L4	3.885244974	1.794547929	-1.114385112	1.19E-44	5.09E-44
DNMT3B	0.214331027	1.713291558	2.998858065	8.89E-49	1.58E-47
ZC3HAV1L	0.278394665	3.208496546	3.52669396	9.33E-49	1.58E-47
TDRD6	0.467583586	0.183224912	-1.351608614	8.20E-32	1.76E-31
TDRD15	0.004529062	0.029177512	2.687572596	0.02202895	0.023879982
TRMT44	2.025023624	0.9335865	-1.117083135	3.00E-44	1.22E-43
NXF5	0.043696744	0.012762909	-1.775568543	7.31E-27	1.37E-26
NXF2B	0.011196804	0.004168956	-1.425328855	5.34E-18	8.19E-18
PIWIL1	0.019712162	0.042348238	1.10321596	2.41E-08	3.06E-08
PIWIL3	0.002699066	0.183789438	6.089449936	5.16E-16	7.63E-16
PEG10	0.945345142	3.060263741	1.69474294	1.35E-22	2.28E-22
ZCCHC3	1.619153771	3.965212831	1.292158299	9.58E-49	1.58E-47
UNKL	3.198639033	1.358594744	-1.235343015	9.87E-47	5.91E-46
SARS2	3.213995727	1.36974769	-1.230457841	4.95E-48	4.10E-47
PAIP2B	3.183617777	0.799412868	-1.993654436	3.25E-45	1.53E-44
RNASE2	0.324312857	0.801765096	1.305793391	1.64E-07	2.04E-07
RNASE4	2.441242333	0.575561332	-2.084573936	1.17E-45	5.71E-45
RNASE6	0.745288791	4.069319799	2.448916197	1.22E-44	5.18E-44
RNASE7	0.16702125	0.046872865	-1.83320678	3.26E-26	5.97E-26
PRR3	1.38838534	3.056135478	1.138300463	4.96E-46	2.55E-45
EIF3C	7.088777004	2.131779616	-1.733478448	8.22E-49	1.58E-47
EIF3CL	4.931912562	1.854052409	-1.411465197	2.75E-48	2.72E-47
HEXIM2	4.015828721	0.996668585	-2.010511978	1.68E-48	2.00E-47
RNPC3	3.858966234	1.084622663	-1.8310212	8.84E-47	5.34E-46
NXT2	0.636738961	2.687074437	2.07726234	1.56E-46	8.90E-46
NXT1	2.234404355	4.800929552	1.103423476	4.68E-48	3.97E-47
PARS2	1.085175452	2.263305292	1.060502882	6.11E-46	3.07E-45
ANKHD1	4.762815841	0.60348746	-2.980419068	8.46E-49	1.58E-47
HELZ2	0.982441525	2.363093631	1.266233347	6.37E-33	1.41E-32
PURG	0.064506123	0.267151179	2.050148371	3.11E-13	4.38E-13
ZC3H14	3.591160674	1.723582089	-1.059040191	8.79E-49	1.58E-47
EZH2	1.303960395	3.256527987	1.320434574	4.83E-47	3.08E-46
ZMAT3	1.084838083	2.550183736	1.233121464	5.12E-45	2.30E-44
PTGES3L-AARSD1	1.580777646	0.052514821	-4.911765987	2.07E-48	2.23E-47
AARSD1	4.883006887	1.485201585	-1.717111052	8.46E-49	1.58E-47
EIF2AK2	1.238501461	3.866143331	1.642299554	1.40E-48	1.80E-47
KHDRBS2	0.102669627	0.760869986	2.889640501	2.26E-18	3.48E-18
KHDRBS3	4.104425969	0.434874149	-3.238510609	2.96E-48	2.83E-47

PTCD2	2.010467959	0.770703074	-1.383284293	1.36E-44	5.76E-44
CPSF4L	0.014661864	0.081140077	2.468346106	8.74E-17	1.31E-16
CSTF2	1.341301645	3.52338065	1.393326624	8.45E-49	1.58E-47
EIF1AY	3.380781565	1.178635524	-1.520239151	5.12E-16	7.59E-16
PPARGC1A	3.259792632	0.139544254	-4.545985569	1.25E-48	1.68E-47
RBM24	6.586879348	0.575815962	-3.515915439	5.69E-48	4.55E-47
LSM11	0.595701473	1.556866924	1.385984201	2.39E-48	2.41E-47
AARS2	1.273584389	3.403394305	1.418079749	7.96E-47	4.87E-46
C9orf129	0.055800119	0.338011458	2.598732041	3.62E-29	7.19E-29
RBPMS	3.789330374	1.111362277	-1.769613751	3.33E-48	3.04E-47
RPL3L	6.877200097	0.308018724	-4.480731365	2.27E-48	2.36E-47
RNASE11	0.017258279	0.004042642	-2.09391832	4.03E-24	7.11E-24
RBM34	4.404344872	0.648324534	-2.764139367	8.47E-49	1.58E-47
ENDOU	0.338696859	0.048377285	-2.807592904	1.17E-38	3.31E-38
EEF1A2	9.883679619	1.842341904	-2.423507423	6.99E-48	5.44E-47
ERI1	1.055642828	2.171540152	1.040596841	1.51E-44	6.39E-44
PRIM1	1.279253378	3.244605879	1.342741202	1.56E-48	1.93E-47
RNASE13	0.128263211	0.028168852	-2.186934762	3.47E-28	6.67E-28
DDX47	4.124975779	0.458589034	-3.169111887	8.46E-49	1.58E-47
HNRNPCL1	0.017858148	0.429416616	4.587723611	5.87E-47	3.68E-46
YRDC	1.895797681	3.866578488	1.02825249	4.80E-48	4.00E-47
SMN1	3.534916364	1.477901158	-1.258126296	1.19E-48	1.63E-47
SMN2	3.58340421	0.956624034	-1.905306846	2.45E-44	1.01E-43
MRPL46	4.52150083	1.379901622	-1.712236313	1.07E-48	1.59E-47
RBM11	0.152199911	0.716722051	2.235446222	5.12E-12	7.03E-12
TSEN2	2.821203226	1.385815224	-1.025575684	1.00E-44	4.34E-44
PTBP3	1.715100897	4.029429902	1.232282285	1.78E-48	2.04E-47
POLR2F	5.324149237	0.038249979	-7.120948255	8.46E-49	1.58E-47
KIAA0391	2.516448471	0.851152672	-1.563899219	3.94E-48	3.48E-47
SNRNP35	4.516887384	2.045142378	-1.143127661	1.14E-48	1.59E-47
TLR7	0.044963747	0.780592034	4.117734557	2.39E-40	7.37E-40
TLR8	0.096035609	0.383452476	1.997406439	4.72E-23	8.08E-23
TLR3	0.245093502	1.130031136	2.204958382	7.21E-34	1.65E-33
BRCA1	0.969120371	2.07944405	1.101450094	3.03E-43	1.11E-42
DQX1	0.070690691	0.161016537	1.187616726	1.93E-05	2.30E-05
CELF3	0.080854957	0.016292398	-2.311137251	3.30E-21	5.41E-21
CELF5	0.040831806	0.148235112	1.860121925	1.16E-19	1.84E-19
CELF6	0.691030062	0.014003903	-5.62484762	8.53E-49	1.58E-47
DDX43	0.184930169	0.569782251	1.62343008	0.000226128	0.000262975
CPEB3	2.216214341	0.720781378	-1.620463776	1.22E-41	4.04E-41
CPEB4	4.409340626	1.79659566	-1.295297177	5.18E-46	2.66E-45
SECISBP2	4.196156442	2.034016841	-1.044736841	8.69E-49	1.58E-47
TARSL2	4.016845717	1.828763203	-1.135194769	2.37E-48	2.41E-47
DDX60	0.895977738	2.10865394	1.234787556	8.87E-37	2.28E-36
PABPC3	0.058777596	2.307116436	5.294680659	9.51E-49	1.58E-47
PABPC4L	0.12237327	1.033897904	3.078733359	1.01E-46	5.99E-46
PABPC5	0.230492013	0.569943253	1.306101527	0.000208676	0.000242946
MEX3A	0.070141857	2.709568986	5.271643949	8.42E-49	1.58E-47
MEX3B	0.594362443	3.492976914	2.555042246	1.07E-48	1.59E-47

MEX3D	0.743231647	4.740879839	2.673270988	8.53E-49	1.58E-47
RBM15B	1.595466855	4.071332454	1.351522395	8.57E-49	1.58E-47
RNASEL	0.731192986	1.580982724	1.112497467	1.55E-38	4.36E-38
RPL39L	0.50417955	3.204650968	2.668157728	2.67E-37	7.03E-37
PARP4	1.701928087	3.542931985	1.057773691	2.53E-47	1.69E-46
FBLL1	0.081742257	0.950783251	3.539962501	4.57E-33	1.02E-32
RPS4Y2	0.003131655	0.173041372	5.788047839	0.000199463	0.000232598
ADAT3	0.759718989	1.741830721	1.197066636	7.59E-29	1.50E-28
RRBP1	3.060207817	8.203740615	1.422652249	9.48E-49	1.58E-47
TERT	0.005753977	0.130204663	4.500077802	0.000204603	0.000238398
PRPF40B	3.607557525	0.472949059	-2.931265695	8.47E-49	1.58E-47
MTO1	3.230817798	1.214360706	-1.411702378	8.80E-49	1.58E-47
POP1	0.745012744	1.951005048	1.388880501	3.15E-46	1.68E-45
YBX2	0.965386142	0.130568673	-2.886297318	2.12E-44	8.75E-44
YBX3	11.36645418	3.476876816	-1.70891841	8.18E-66	1.17E-62
TRIM21	1.465016117	3.438787191	1.230983302	1.88E-46	1.05E-45
RNASEH2A	1.983534604	4.879527576	1.29866791	8.80E-49	1.58E-47
ESRP2	0.316238038	0.141161067	-1.163668669	3.40E-22	5.69E-22
NOL9	1.940885713	3.954572974	1.026806748	1.67E-48	2.00E-47
ARL6IP4	6.540055119	1.123189244	-2.54170177	8.35E-49	1.58E-47
CNOT6	1.402176443	3.016215803	1.105071751	8.56E-49	1.58E-47
LRRFIP2	5.273395586	2.610275915	-1.014529913	8.79E-49	1.58E-47
EIF4E3	3.947752103	1.196814111	-1.721832308	1.92E-48	2.14E-47
CTU1	0.97681414	2.820855321	1.529976684	2.83E-45	1.33E-44
PAPOLB	0.012005947	0.03787917	1.657655552	1.41E-09	1.83E-09
EXO1	0.082003568	2.121775008	4.693441184	8.43E-49	1.58E-47
NANOS1	2.84443457	0.644152852	-2.142666923	9.23E-43	3.26E-42
NANOS3	0.124930643	0.540725018	2.113767718	1.06E-28	2.07E-28
IFIT2	0.561795714	2.996590735	2.415204536	6.18E-46	3.09E-45
IFIT5	0.825903533	2.86576777	1.794876516	9.70E-49	1.58E-47
IFIT1B	0.016860515	0.074371132	2.141094133	1.32E-09	1.71E-09
IFIT3	1.420274657	4.205928884	1.566254507	1.02E-45	5.00E-45
NOVA1	1.603217201	0.324608882	-2.304195512	8.04E-39	2.30E-38
SARNP	5.122560369	0.767995517	-2.737695286	8.46E-49	1.58E-47
SRRM4	0.09865664	0.040877731	-1.271101042	3.83E-21	6.26E-21
LIN28A	0.004774558	0.099652335	4.383464525	1.15E-22	1.95E-22
RBM4	5.031064854	2.313077717	-1.121050047	8.46E-49	1.58E-47
SF3B4	3.091841362	6.493246263	1.070473628	8.47E-49	1.58E-47
BAZ2B	3.004158039	0.9232339	-1.702192605	9.13E-49	1.58E-47
JAKMIP1	0.057005578	0.133162718	1.22401522	4.76E-06	5.74E-06

Supplementary Table 5. Clinical utility of the hub RBPs

id	gender (Female, Male) t(p)	age (≤ 20, > 20) t(p)	M Stage (M0, M1) t(p)
YRDC	4.239 (0.237)	1.568 (0.140)	-2.177 (0.039)
ZC3HAV1	2.22 (0.528)	-1.414 (0.177)	0.352 (0.727)
TERT	1.554 (0.670)	2.68 (0.009)	-0.581 (0.564)
RBM34	5.782 (0.123)	2.134 (0.045)	-1.127 (0.265)
TLR8	5.471 (0.140)	-1.221 (0.245)	1.719 (0.092)
IGF2BP2	4.972 (0.174)	-0.784 (0.449)	-1.747 (0.089)
NXT2	0.808 (0.847)	-1.309 (0.214)	2.079 (0.046)
RRPS-score	2.856 (0.414)	1.91 (0.062)	-1.712 (0.101)

t: t value from Student's t test; p: *p*-value from Student's t test.

Supplementary Table 6. Identification of DEGs between the high and low RRPS-score subgroups

gene	lowMean	highMean	logFC	*p*Value	fdr
FPR1	1.464175536	0.812055778	-0.850437794	9.37E-05	0.007909171
VPS9D1-AS1	1.365149985	2.216834845	0.699441828	0.002398811	0.042319314
VAV1	1.53521417	0.980243758	-0.647227478	0.000167378	0.010523421
TLR2	1.801954638	1.271224325	-0.503344058	0.000499155	0.017824807
AL022322.1	1.036422424	1.852216726	0.837640782	0.000593759	0.019825513
SASH3	2.144799619	1.372525472	-0.644009944	2.73E-05	0.00424863
ARHGAP9	1.709007799	1.120265668	-0.609318077	6.54E-05	0.007026378
CFI	2.621716508	1.65603092	-0.662782083	0.000433694	0.016222351
COL24A1	2.013830539	3.117656766	0.630519818	6.03E-05	0.006723781
AL513534.1	1.344205064	1.973981657	0.55435534	0.002681818	0.044461923
CGREF1	2.521485346	3.808733824	0.595037627	0.000202065	0.01128613
MLC1	1.80730913	3.047081755	0.753584917	0.001321749	0.032014491
ZBED6	0.932142703	1.410511095	0.597595274	0.002003892	0.038957237
KCNMA1	1.120965007	1.694394484	0.596028556	0.003053501	0.047117995
AL035446.1	2.211194931	1.356656719	-0.704770499	0.001440832	0.033597697
ITGBL1	1.44120617	0.828754633	-0.798259798	0.001933181	0.038147238
REEP1	1.426409663	2.128408124	0.577386434	0.001502521	0.0340879
LRRC25	2.344322585	1.614342569	-0.538224347	9.37E-05	0.007909171
PCED1B	1.338661086	0.78612706	-0.767956338	4.16E-05	0.00553082
NCF4	2.654524858	1.742609977	-0.607203944	7.20E-06	0.002432503
AL928654.2	1.03091595	1.511744725	0.552287829	0.000754044	0.023090164
LTB	1.459214499	0.713088685	-1.033038553	0.000123176	0.00893212
C1S	3.775652209	2.660193842	-0.505194503	0.001502521	0.0340879
BX322562.1	1.483088701	0.99776585	-0.571831689	0.003053501	0.047117995
F13A1	3.235605679	2.082736371	-0.635555561	0.000217721	0.011592168
CD52	2.415150527	1.408442648	-0.778012292	0.00026448	0.012971616
ALOX5AP	2.818081363	1.894473017	-0.572916674	8.65E-05	0.007900393
ANP32BP1	0.925181909	1.343682847	0.538383694	0.000202065	0.01128613
CORO1A	2.77931774	1.893234508	-0.553877654	3.91E-06	0.001849019
HCST	2.511225343	1.618346938	-0.633870571	0.000922061	0.025887801
PRF1	1.316385977	0.743059435	-0.825033045	0.000681026	0.021523343
HPGDS	1.346736804	0.938993939	-0.520280179	0.00262775	0.043932111
IL10RA	1.983237169	1.335289272	-0.570704899	0.000834183	0.024527481
CCL2	2.477028655	1.541086205	-0.684662993	0.001199439	0.030423537
CSAG1	2.423806574	1.056331406	-1.198212045	0.000202425	0.01128613

NKG7	2.04635306	1.10186616	-0.893106082	0.000180529	0.010722867
HGF	1.487047934	0.794617233	-0.904119166	0.000681026	0.021523343
PTPN7	1.198226572	0.805623558	-0.572722956	0.000985272	0.026588838
DLGAP1-AS1	1.252907232	0.858491618	-0.545403644	4.91E-05	0.006050886
BATF	2.005696971	1.242599753	-0.690741982	0.000363012	0.014694507
HPDL	1.179930959	1.973060994	0.74173311	0.000124649	0.008983856
ARHGAP44	1.097099328	1.77887112	0.697267841	0.000475857	0.017413718
HK3	1.463168235	0.901381697	-0.6988856	0.000123176	0.00893212
GIMAP1	1.313042452	0.877201387	-0.581933563	0.001502521	0.0340879
MUC1	1.018247177	1.677071168	0.719856098	0.000418616	0.015961405
ITGAM	1.921946096	1.219382323	-0.656417337	5.79E-05	0.006708834
VSIG4	3.401289788	2.020892435	-0.751089394	1.42E-05	0.003251779
COCH	0.675402879	2.029683335	1.587434427	2.30E-05	0.004120197
AC010609.1	0.770220581	1.764466837	1.195888736	0.001521202	0.034445616
GPRC5A	0.699484582	1.453889194	1.055553156	0.000834183	0.024527481
SIGLEC1	1.93466971	1.263922756	-0.614178992	0.00218807	0.040489231
IGF2BP2	2.092563936	3.345793398	0.677076659	1.14E-06	0.001474361
SELL	2.024016121	1.350248428	-0.583995913	0.00136498	0.032660048
MAGEA12	2.172157234	0.998262412	-1.121637528	0.001299525	0.031934281
TRIM17	0.962885067	1.644498776	0.772212426	0.002121642	0.039932825
AL161909.1	1.056386841	1.919624161	0.861685641	7.09E-05	0.007349172
CHML	1.67832073	2.426730631	0.531995533	0.001123737	0.029128442
CSAG3	1.630431191	0.797104947	-1.032411968	0.001899639	0.038057179
IHH	0.580456871	1.809832316	1.640595254	0.000133683	0.00924056
DDN	0.811375813	1.383021096	0.769380961	0.001502521	0.0340879
ZFPM2-AS1	1.400597864	0.940745581	-0.57416628	0.001601102	0.035046351
RASSF4	2.3270187	1.626574749	-0.516645682	0.000167378	0.010523421
FKBP1B	1.467622464	0.990718038	-0.566934467	0.000614555	0.020177882
CDA	1.335770411	0.826241262	-0.693037048	0.000573612	0.019539183
IL2RG	2.156676585	1.511099327	-0.513211352	0.002326607	0.041541526
RPS3P6	1.186094522	1.758542269	0.568161027	0.003240537	0.048608062
LINC02593	1.401200199	2.183081526	0.63970291	0.002256376	0.040780365
AC090559.1	1.474294653	1.021356521	-0.52953834	0.000985272	0.026588838
ABLIM3	1.638680964	1.091741551	-0.585903636	1.14E-05	0.002920046
CITED4	1.625631281	2.324886786	0.516160395	0.001601102	0.035046351
MIR4664	0.766667369	1.676660201	1.128917654	0.002214076	0.040780365
CHN2	1.351105516	2.071549923	0.616570241	0.000303106	0.013886499
FAT3	2.32266397	3.57885753	0.623718664	1.04E-05	0.002789332
HOMER2	1.89279857	2.73502899	0.531035236	0.000593759	0.019825513
IGHG3	1.561268131	0.515400846	-1.598951516	0.001872601	0.037667619
NCF1C	1.441195059	0.877981573	-0.715003044	0.002256376	0.040780365
NGEF	1.569415656	2.427535298	0.629264776	0.001760038	0.036370011
CASP1	1.987685776	1.353726956	-0.554152926	0.000180529	0.010722867
LILRB4	2.074663834	1.298078935	-0.676499475	0.000118489	0.008864153
HSD3B7	2.53977184	1.751402079	-0.536188569	0.000376234	0.014973341
CXCL13	2.007219443	1.107733811	-0.857587109	0.001439282	0.033597697
COL13A1	2.211904196	3.203703343	0.534451663	0.000271698	0.013001881
GZMB	1.367356723	0.945206627	-0.53268802	0.001397433	0.033121763
AL139393.2	1.722473372	2.437664678	0.501018004	0.00270834	0.044461923

LOXL4	2.051855077	2.935913363	0.516880559	0.003053501	0.047117995
CD48	1.489460416	0.845113324	-0.817573068	6.03E-05	0.006723781
ANO5	2.699321698	4.222626264	0.645543639	7.68E-05	0.007564778
RTP4	1.467497604	0.949370543	-0.628314956	0.002398811	0.042319314
HLA-DQA2	2.378360844	1.453442668	-0.710493453	0.002791157	0.045255794
IGHA1	2.79737048	1.312440646	-1.091819155	0.002254396	0.040780365
RENBP	3.264038203	2.262779184	-0.528562139	1.62E-05	0.0033073
LINC02298	1.19532447	1.755798662	0.55472513	0.00270834	0.044461923
KBTBD11	1.12091908	1.656996278	0.563888229	0.001601102	0.035046351
AMIGO2	1.603732048	0.929404878	-0.787053994	0.000985272	0.026588838
TMEM273	1.557180833	0.856962787	-0.861632029	0.000325877	0.014266156
AC124798.1	1.135020526	1.697167376	0.580410465	9.37E-05	0.007909171
PANX3	4.172074974	6.308796198	0.596599662	0.000118489	0.008864153
LURAP1L	1.325739783	0.826745092	-0.681283149	0.00181612	0.037075196
NDNF	2.929763538	4.428843944	0.596145934	1.93E-05	0.003571884
HLA-DRB6	2.519015422	1.638663997	-0.62033989	0.001455332	0.033597697
LINC01711	1.462348588	0.875311628	-0.740418615	0.003372584	0.049829926
LY86	2.328489238	1.542490933	-0.594132205	4.34E-05	0.005638801
CACNA2D4	1.486786114	0.979991972	-0.601355284	0.001018342	0.027232576
PTGER4	1.754106158	1.218617088	-0.525491187	0.001873821	0.037667619
GALNT14	2.309134984	3.414790772	0.564444675	0.000465365	0.017082636
LINC00960	0.761485644	1.262567447	0.729471716	0.000922061	0.025887801
MYOM2	0.744665751	1.371680643	0.881279719	0.000985272	0.026588838
IFI30	1.257706307	0.860230587	-0.547999737	0.003240537	0.048608062
AL109936.2	0.804190387	1.234361455	0.618155921	0.003145767	0.048040008
SLC8A3	1.749830809	2.822833706	0.689928707	0.002057048	0.039279984
HSPA4L	0.771616946	1.23668442	0.680520664	0.001255778	0.031249055
S100A9	3.265037462	1.928054774	-0.759953507	7.38E-05	0.00745414
AC019129.1	0.950491074	1.668518323	0.811822546	3.38E-05	0.004868638
AL031847.1	0.717340033	1.302439008	0.860486763	0.003185049	0.04857713
PLCB4	1.473763319	2.293204316	0.637860047	1.49E-05	0.003251779
SMPD3	2.359777287	3.747732166	0.667367147	0.000704611	0.021917101
SLC16A8	0.976410676	1.742677165	0.835745357	0.00127977	0.031514331
LPAR5	1.789388214	1.162282893	-0.622505163	7.99E-05	0.007681045
PTCH1	1.484988254	2.140114495	0.527236462	0.000314301	0.014179526
LYL1	1.762129413	1.243883727	-0.502468247	0.000243326	0.012186909
MAGEA3	3.09797106	1.74008595	-0.832165099	0.001342905	0.032460407
LPAR3	1.040660084	2.157245489	1.051691449	7.92E-05	0.007681045
TMEM150B	1.238684755	0.790277383	-0.648378043	0.002398811	0.042319314
MS4A4A	2.604060083	1.724106479	-0.594913859	0.000202065	0.01128613
SMAD9	1.791626495	2.544024144	0.505842456	0.000389899	0.0152603
ERAP2	2.84162373	1.886963326	-0.590649151	0.002963682	0.046645433
CD163	3.282718751	2.193337482	-0.58176334	7.68E-05	0.007564778
AL645608.6	1.274855209	2.019107718	0.663384477	0.002188885	0.040489231
SPICE1	1.219325405	1.726508542	0.501774278	6.81E-05	0.0071852
AL645608.4	0.781111024	1.510098079	0.951042727	0.001768205	0.036475024
RTN3P1	0.981707724	1.41696169	0.529435281	0.002549332	0.04341946
AC117402.1	2.452698977	1.243015268	-0.980526163	0.001675721	0.035752758
LILRB2	1.531094469	0.943093976	-0.699089857	0.000404022	0.015606342

APOL3	1.975182237	1.388057992	-0.508917923	0.001933181	0.038147238
MMP19	2.268214453	1.536968651	-0.56146931	0.002473036	0.043113988
AL161785.1	1.391531303	0.892006004	-0.641548037	0.001650652	0.035322519
FCGR1A	1.67892489	0.924999215	-0.860013643	1.36E-05	0.003213346
COL11A2	3.411547772	5.743774189	0.751572614	9.77E-07	0.001474361
CEBPA	2.395826669	1.653187263	-0.535273383	9.37E-05	0.007909171
AC022868.1	0.896504725	1.299863467	0.535977004	0.001994242	0.038833515
GGT1	1.372079703	0.886034422	-0.630929636	0.003053501	0.047117995
SYDE2	0.863141191	1.340864233	0.63549469	9.92E-06	0.002789332
PARVG	1.394113535	0.834138468	-0.74098926	2.93E-06	0.001822471
RPS3AP25	0.888769108	1.31064018	0.560391088	0.000167378	0.010523421
IRF5	1.377763139	0.970958503	-0.504846343	0.000516885	0.018183264
IL17RB	0.990277019	1.57513978	0.669575796	0.000598129	0.019915156
RPS27P21	0.978208718	1.429212175	0.547005882	0.002321007	0.041541526
NFAM1	1.646935799	1.115395894	-0.562228452	0.000173838	0.010722867
GJA5	1.855832459	1.190898142	-0.640016449	0.001199439	0.030423537
PODN	2.403017527	1.444620646	-0.734156477	4.52E-05	0.005751042
ITGA3	1.905897724	1.340273655	-0.507943105	0.001409496	0.033121763
AC006329.1	0.690274266	1.398782002	1.018929532	0.002220588	0.040780365
MSC	3.277452864	2.248001636	-0.543931946	0.001705534	0.03587083
CXCL12	2.741361793	1.840720042	-0.574622519	0.001601102	0.035046351
CRYBG1	2.14823418	1.445033118	-0.572048713	5.34E-05	0.006306124
PYCARD	2.734239744	1.879149859	-0.541059623	7.20E-06	0.002432503
LST1	2.014828988	1.302735628	-0.629113054	0.000325877	0.014266156
PAGE5	2.895581127	1.155402639	-1.325457223	8.69E-05	0.007900393
NCR3LG1	0.891802017	1.70122487	0.931778483	1.03E-06	0.001474361
MAGEA6	2.784442985	1.545286991	-0.849513951	0.002562184	0.043575566
CD36	2.264405061	3.246785892	0.519880196	0.000314301	0.014179526
ADGRD1	0.953674121	1.616022018	0.760878581	0.00264565	0.044168908
CA3	3.593827364	5.453758978	0.601729836	0.001199439	0.030423537